

出國報告(出國類別：研習)

「移動污染源PM_{2.5}檢測技術」研習
出國報告

服務機關： 行政院環境保護署環境檢驗所

姓名職稱： 李其欣科長

派赴國家： 美國

出國期間： 103年10月16日至10月31日

報告日期： 104 年 1 月 5 日

「移動污染源 PM_{2.5} 檢測技術」研習

摘要

本次出國計畫至美國研習，主要參訪美國環保署研究三角園區（U.S. EPA Research Triangle Park）實驗室，該實驗室為美國環保署建置空氣中細懸浮微粒（PM_{2.5}）相關檢測技術之研究單位，本計畫希望藉由觀摩先進國家量測技術開發實務經驗，以作為未來相關管制法規及檢測技術、方法建立之參考。

本次參訪研習內容包括：移動污染源PM_{2.5}量測技術使用之檢測方法、儀器設備需求、採樣限制及環境干擾、量測天平室之環境條件規範，以及檢測結果之數據解析等相關議題探討。在美國環保署研究三角園區之研習過程中，不但可學習移動污染源檢測技術，並可觀摩美國環保署對於交通空氣污染物的監測設計，以及空氣中細懸浮微粒污染源建訂技術，並與三角研究園區的資深研究人員充分討論檢測實務執行上可能面臨問題及解決方法，研習計畫成果可提供未來國內研訂空氣污染管制規範，建立相關檢（監）測技術或研擬檢測方法之參考。

本研習計畫提出建議：一、黑碳檢測技術可提供國內移動污染源PM_{2.5}檢測技術研發之參考，但需注意儀器設備適用濃度的限制，以及檢測結果穩定性。二、以SEM-EDX同時檢測粒狀物的巨觀形狀與微觀的元素成分，可作為污染物來源判定的分析技術，建議可提供國內發展環境污染來源鑑定技術之參考。三、U.S. EPA RTP移動污染源空氣品質測站同步監測空氣品質與交通流量，並進行資料比對，其構想可提供國內進行環境調查、監測規劃時之參考。四、美國環保署對於空氣中粒狀物檢測，也重視PM₁₀的相關議題。對於國內空氣中粒狀物之檢測技術發展，建議可進行PM₁₀相關議題研究。

目次

壹、目的.....	3
貳、行程.....	4
參、研習過程.....	5
肆、心得及建議.....	21
伍、附件	23

壹、目的

目前國內交通工具所造成的污染排放問題，造成都市的空氣污染日益嚴重，尤其是在交通尖峰時段。而對於移動性污染源的法規管制的管制項目（包括：粒狀污染物（PM）、一氧化碳（CO）、碳氫化合物（C_xH_y）、氮氧化物（NO_x）等），是否足以達到管制目標及需求，仍有許多研究調查工作正在進行，以尋求解決之道。

本計畫經由國立臺灣大學公共衛生學院職業醫學與工業衛生研究所陳志傑教授引介，取得任職於美國環保署研究三角園區陳福麟先生之聯絡資料，經多次與陳先生溝通聯繫，並取得美國環保署研究三角園區安全管理主管、國家風險管理研究實驗室（National Risk Management Research Laboratory）主管及國家暴露研究實驗室（National Exposure Research Laboratory）主管同意前往該等實驗室參訪，方能使本計畫得以順利進行。

本次參訪美國環保署研究三角園區研習的技術包括：車輛行車型態污染排放檢測技術、黑碳（Black Carbon）檢測技術、交通空氣品質監測設備及技術、空氣中細懸浮微粒（PM_{2.5}）被動採樣技術、細懸浮微粒檢測技術（電子顯微鏡及能量分散式X-射線檢測儀，SEM-EDX）、美國國家風險管理研究實驗室近期執行的研究計畫說明及觀摩細懸浮微粒分析實驗室設施及檢測設備等。。

本計畫研習行程，除參訪美國環保署研究三角園區內的2個研究部門，並前往美國環保署設於北卡羅萊納州I40高速公路旁的交通空氣污染監測站，相關研習之技術，有助於提昇國內移動行污染源細懸浮微粒之檢測技術，並可提供日後修訂空氣污染防制法規與研訂檢測方法之參考。

貳、行程

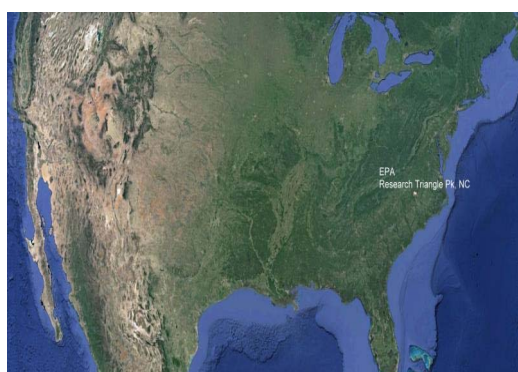
時間	行程	活動地點
10月16日(四) 17:30 臺灣出發	臺灣出發前往美國	去程
10月17日(五) 20:15(美國時間)	抵達紐約	紐約
10月18日(六)	相關資料蒐集及聯絡參訪行程	紐約
10月19日(日)	紐約出發前往北卡羅萊納州羅利達拉姆	北卡羅萊納州
10月20日(一) 至 10月24日(五)	參訪美國環保署三角研究園區(U.S. EPA RTP)實驗室及移動污染源 PM _{2.5} 檢測技術研習	北卡羅萊納州
10月25日(六)	相關資料蒐集	北卡羅萊納州
10月26日(日)	相關資料蒐集	北卡羅萊納州
10月27日(一) 至 至10月28日 (二)	參訪美國環保署三角研究園區(U.S. EPA RTP)實驗室及移動污染源 PM _{2.5} 檢測技術研習	北卡羅萊納州
10月29日(三)	由羅利達拉姆出發前往紐約	紐約
10月30日(四) 22:50(美國時間)	紐約出發返回臺灣	返程
10月31日(五)	經國際換日線	返程
11月1日(六) 06:00(臺灣時間)	抵達桃園機場	返程

註：美國與臺灣時差為-12 小時

參、研習過程

(一) 參訪行程安排及確認會議

本次出國研習計畫在到達美國環保署位於北卡羅萊納州教堂山市 (Chapel Hill) 的研究三角園區 (簡稱U.S. EPA RTP) 實驗室後，即由美國環保署研究三角園區的研究人員陳福麟先生邀集Richard W. Baldauf博士與Thomas Long工程師，討論參訪行程的安排及確認技術研習內容包括：車輛行車型態污染排放檢測技術、黑碳 (Black Carbon) 檢測技術、空氣中細懸浮微粒被動採樣技術、細懸浮微粒檢測技術 (電子顯微鏡及能量分散式X-射線檢測儀，SEM-EDX)、移動污染源空氣品質監測技術、美國國家風險管理研究實驗室近期執行的研究計畫說明及觀摩PM_{2.5}分析實驗室設施及檢測設備等。



U.S. EPA RTP地理位置圖

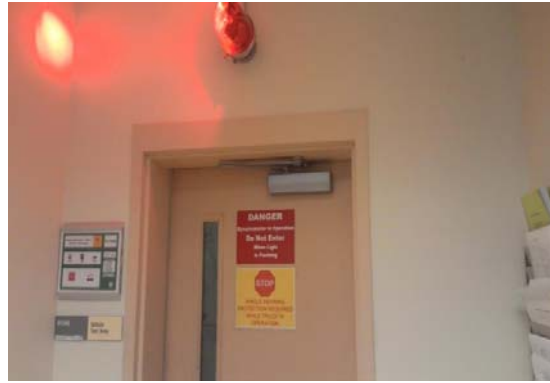
(二) 車輛行車型態污染排放檢測技術研習

U.S. EPA RTP為美國空氣污染物檢測技術的研發單位，美國環保署空氣品質及車輛污染物排放之標準檢測方法，大都由此單位開發及驗證。因此，本計畫於參訪U.S. EPA RTP國家風險管理研究實驗室時，即觀摩該實驗內的車輛行車型態污染排放檢測設備，並請其研究人員進行實測作業。

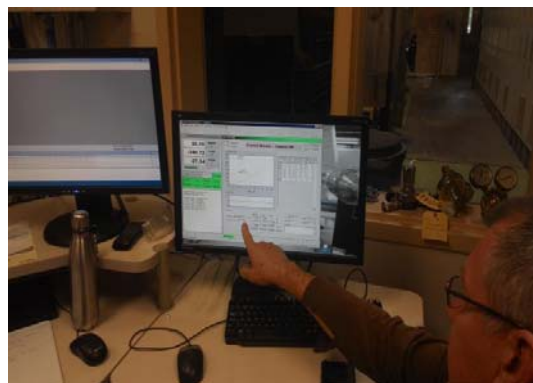
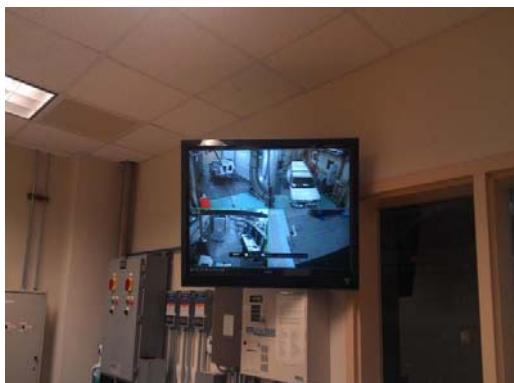
觀摩該實驗室之車輛行車型態污染排放檢測設備時，發現其檢測設備

大致上與國內機動車輛測定機構之檢驗測定設備相同，測定項目包括：碳氫化合物（C_xH_y）、氮氧化物（NO_x）、一氧化碳（CO）、粒狀污染物（PM, Particulate Matter）。

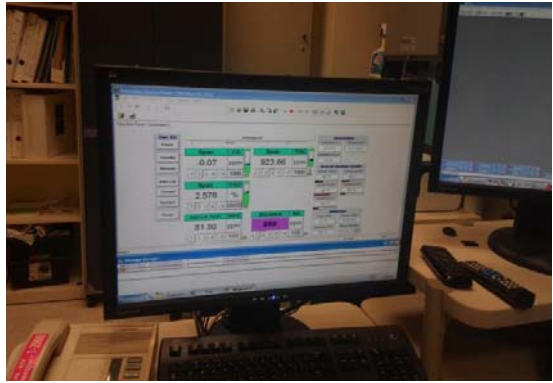
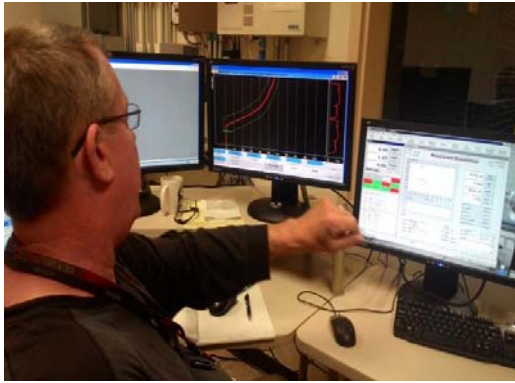
另亦發現該實驗室對於測試人員及環境的安全問題相當重視，如：測試過程均以錄影設備監視、測試時以警示設備管制人員進出、設置各種危害性氣體監測設備等，可提供國內機動車輛檢驗測定實驗室測試環境規劃之參考。



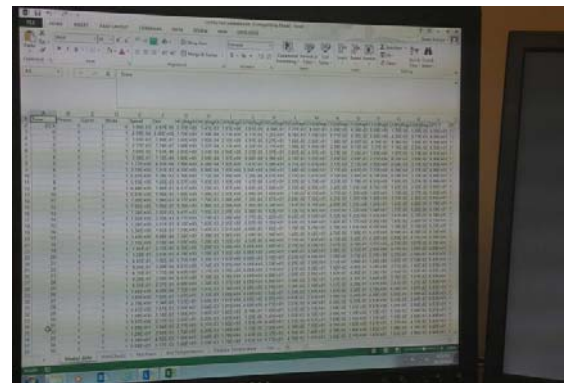
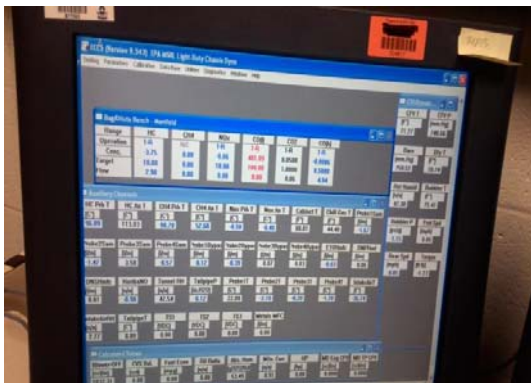
車輛行車型態污染排放檢測實驗室



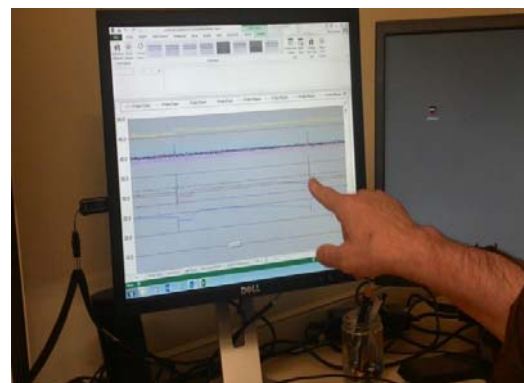
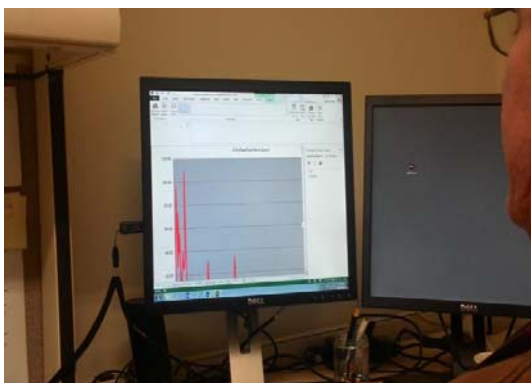
車輛行車型態污染排放檢測作業



車輛行車型態污染排放檢測作業



車輛行車型態污染排放檢測數據



車輛行車型態污染排放檢測結果



車輛行車型態污染排放檢測－裝填PM樣品濾紙



車輛行車型態污染排放檢測－取出PM樣品濾紙



車輛行車型態污染排放檢測－PM樣品收集

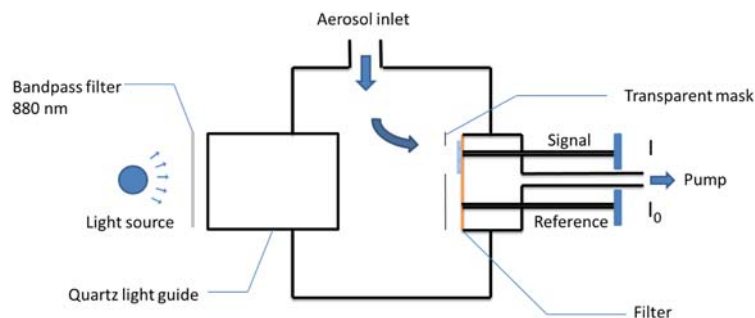
(三) 黑碳 (Black Carbon) 檢測技術研習

國內對於移動污染源細懸浮微粒（PM_{2.5}）之檢測技術研發，目前實務執行上仍有許多關鍵技術待克服，此次參訪U.S. EPA RTP國家風險管理研究實驗室，發現該實驗室有使用黑碳檢測儀進行研究計畫，對於國內正在發展的移動污染源PM_{2.5}檢測技術所面臨瓶頸，似乎出現解決問題的契機。

移動污染源PM_{2.5}中成分大部分為黑碳，因此該實驗室以黑碳檢測儀（microAeth® Model AE51）檢測之，可檢測黑碳的濃度範圍為0-1 mg BC/m³，偵測極限為0.1 μg BC/m³，解析度為0.001 μg BC/m³，氣體流率可調整為50、100、150或200 ml/min，檢測結果可設定每1、10、30、60或300秒出具一筆數據，並可藉由USB連接電腦電腦下載數據及提供電源。

黑碳量測儀係利用黑碳會吸收光的原理，量測濾紙上黑碳的含量。以發光二極體為光源，經由光柵篩選波長為880 nm的光徑，穿透石英導光器後，穿透過濾紙，以偵測器偵測光強度。於濾紙前方設一個遮蔽器，其可讓光通過，但會阻斷氣流，並留一個直徑5 mm的缺口，而讓微粒沉積在遮蔽器缺口。然後以遮蔽器缺口處量測到的光強度I，而濾紙上沒有微粒沉積部分的光強度為I₀，依下列公式計算光衰減量（A）。

$$A = 100 \ln(I_0/I)$$



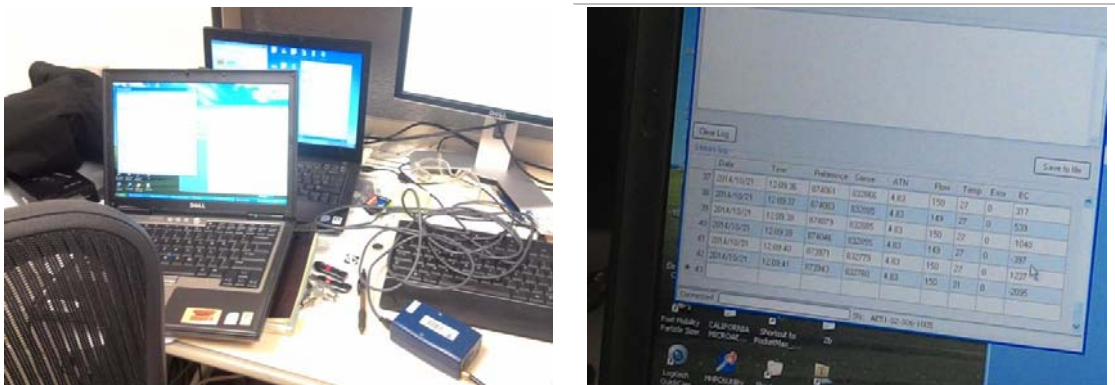
黑碳檢測儀內部構造圖

由光衰減量與黑碳濃度的關係式，但當黑碳濃度超過一定濃度時，儀

器會產生不靈敏情形。另外當濾紙存在黑碳以外之干擾物時，亦會造成檢測上的誤差。以現場測試結果，每秒檢測數據變動很大，建議可建立儀器的校正步驟，並進行驗證試驗，以確認其可運用於移動污染源PM_{2.5}檢測。



黑碳檢測儀



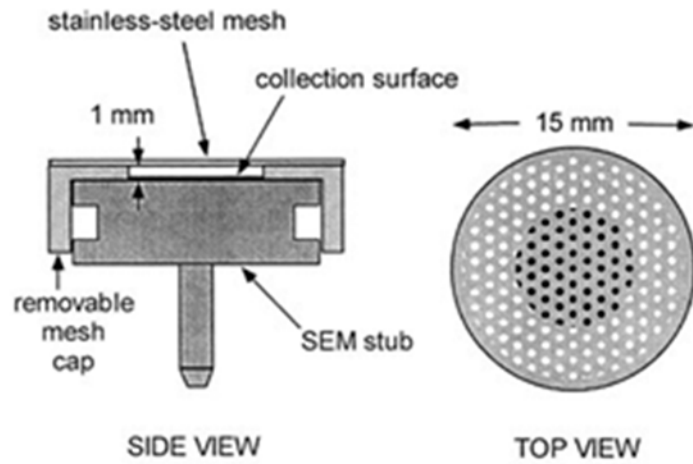
黑碳檢測儀連接電腦即時檢測

(四) 空氣中細懸浮微粒被動採樣、檢測技術

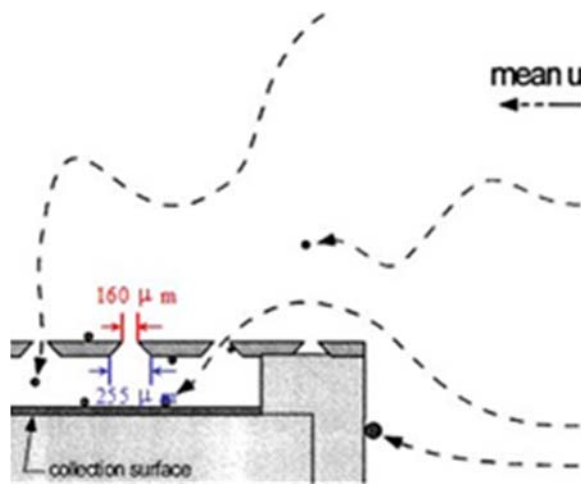
空氣中PM_{2.5}被動採樣與檢測技術是由U.S. EPA RTP國家暴露研究實驗室 (National Exposure Research Laboratory, NERL) 的Willis, Robert 博士負責研發，採樣器的構造是由PM_{2.5}樣品承接盤與不鏽鋼上蓋結合而成，不鏽鋼上蓋的直徑為15 mm，上有布滿孔徑160 μ m的篩孔，將結合後的採樣器裝設在具有上下層承接盤之下層的中央位置，然後固定放置於採樣點後

即可進行採樣。採樣時間通常為14天，但可依收集到的樣品量調整採樣時間。

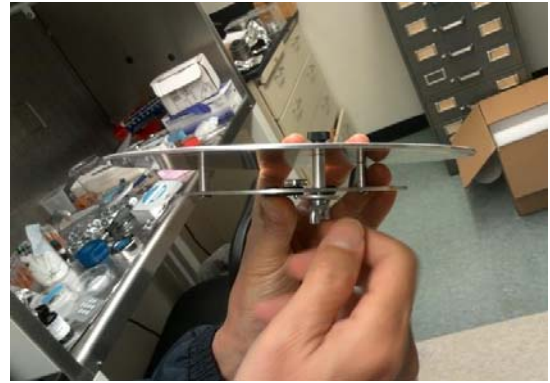
採集的PM_{2.5}樣品在U.S. EPA RTP NERL係以SEM-EDX檢測，可同時觀察每個粒狀污染物的外觀及檢測其所含元素成分，以同步檢測污染物的巨觀與微觀分析結果，可提供環境污染源鑑定技術建立之參考。



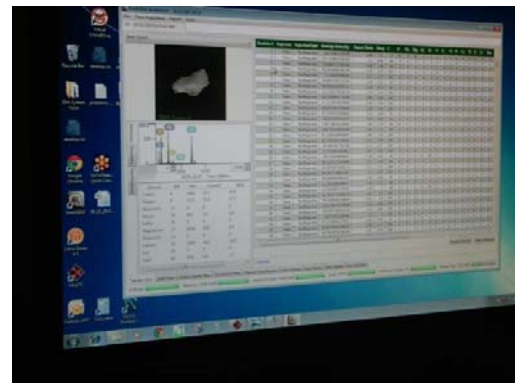
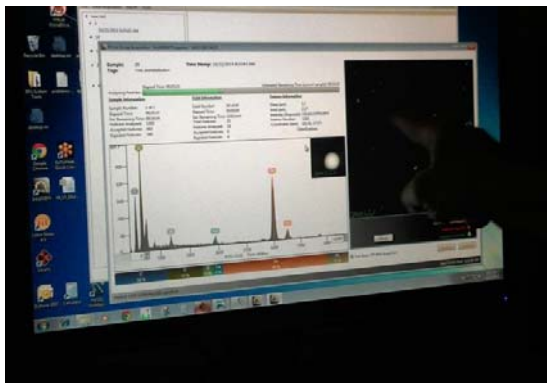
PM_{2.5}被動採樣器結構圖



PM_{2.5}被動採樣示意圖



PM_{2.5}被動採樣器



PM_{2.5}被動採樣檢測結果原始數據



PM_{2.5}被動採樣檢測數據分析

(五) 移動污染源空氣品質監測技術

本計畫行程參訪U.S. EPA RTP設置於I40高速公路旁的移動污染源空氣品質監測站，此測站與國內空氣品質測站相同的地方，共同的監測項目PM_{2.5}、NO_x、O₃及CO，但此測站還具備超細懸浮微粒（PM₁）監測儀與雷達即時偵測交通狀況，並將即時監測的結果都儲存至電腦，可同步分析空氣污染物濃度變化與交通流量的關係，可提供國內移動污染源空氣品質監測規劃之參考。

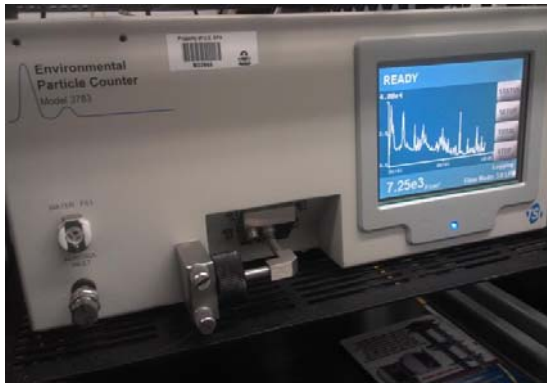
另對於PM₁的檢測技術，已運用於此測站，可見U.S. EPA RTP對於PM₁亦有進行研究，目前國內對於此方面的研究議題較少，對於空氣中粒狀物的探討，PM₁相關之研究將成為未來發展的方向。



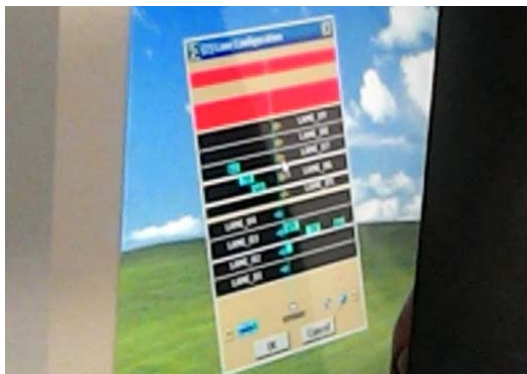
移動污染源空氣品質監測站



移動污染源空氣品質監測站-NO_x、O₃監測儀



移動污染源空氣品質監測站-PM₁及雷達監測



移動污染源空氣品質監測站-監測數據分析

(六) 觀摩PM_{2.5}分析實驗室設施及檢測設備

本次參訪U.S. EPA RTP國家風險管理研究實驗室時，也觀摩該實驗室中PM_{2.5}分析的實驗室設施及檢測設備，實驗室設有控制天平室環境條件（包括：溫度、溼度、潔淨度）的控制設備24小時運轉，並留有監控紀錄。天平室內除了有一套手動秤重天平外，還有一套自動秤重設備。

經比較發現本所天平室的環境條件控制設備，只有當有樣品時才啟動，就其原因係考量本所主要的PM_{2.5}樣品來自本署環境監測及資訊處的空氣品質監測站以及本所的研究調查計畫，可掌控其檢測期程，惟對於突發事件的樣品，可能產生無法及時因應之情況。在考量天平室環境條件控制設備運轉所耗費的電力成本亦是龐大的支出，經權衡僅能將PM_{2.5}樣品儘量集中

分析。



天平室環境條件控制設備及樣品調理



手動秤重天平及自動秤重設備

(七) 美國國家風險管理研究實驗室近期執行的研究計畫

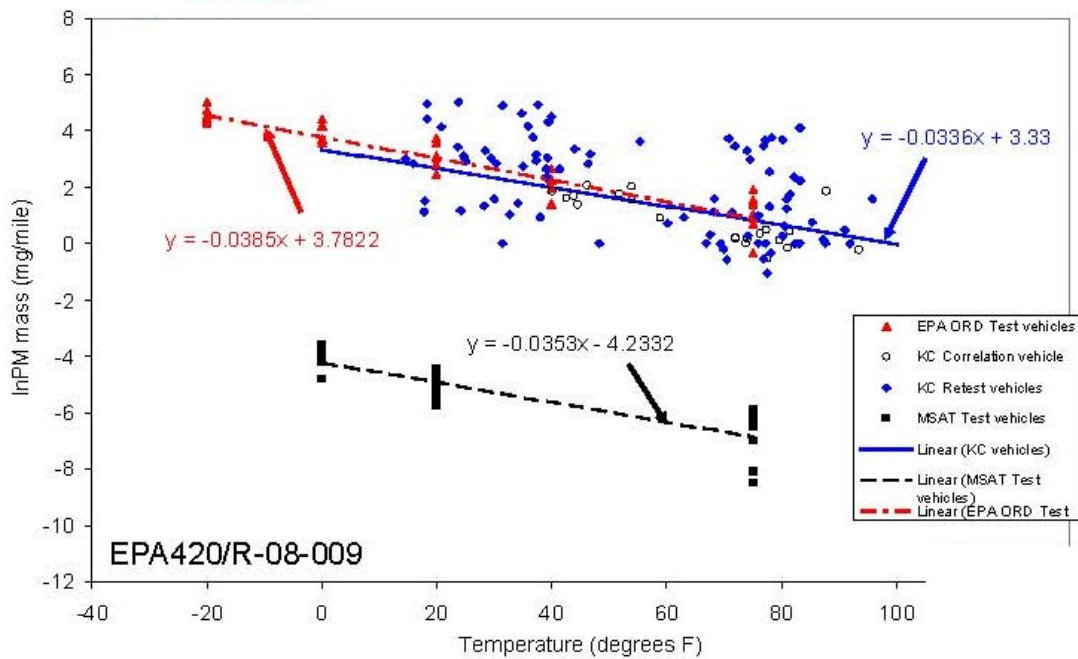
本計畫參訪期間，在U.S. EPA RTP 國家風險管理研究實驗室的Richard W. Baldauf博士熱心的協助下，方能使得參訪行程順利進行，而且Richard W. Baldauf博士也很大方的安排一個下午的時間解說該實驗室近期所執行的研究專案。

美國國家風險管理研究實驗室近年來主要的研究議題為交通工具污染排放及鄰近污染源的衝擊 (Transportation Emissions and Near-Source Impacts)，研究內容包括汽車排放污染物特性、鄰境道路的空氣品質及健

康效應、飛機引擎排放污染物、港口及鐵路產生的污染物及暴露效應等。

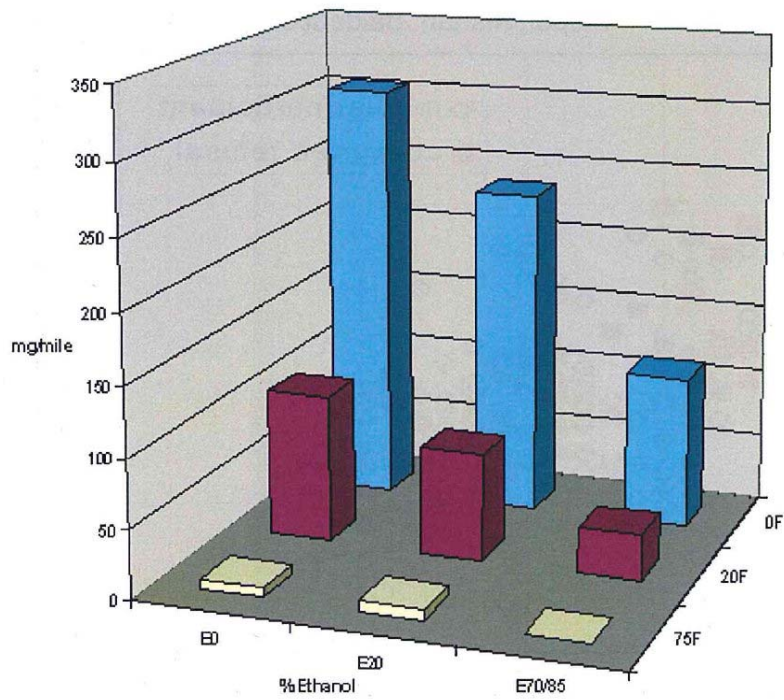
由交通工具排放產生的空氣污染物有：CO、NO_x、Pb、毒性氣體（如：苯、甲醛等）及粒狀物（PM_{2.5}、PM₁₀、有機物、金屬物等）。實驗室可檢測及控制交通工具所排放的污染物質，並經由實地與實驗室檢測污染排放情形，以及污染對空氣品質的影響，分析項目包括粒狀物、揮發性有機物，並研究污染物的排放、散布模式及大氣的反應。

經研究探討檢測時之大氣溫度與交通工具排放粒狀物之關係，可發現當進行測試時大氣溫度越低時，顯示排放的粒狀污染物有偏高趨勢。

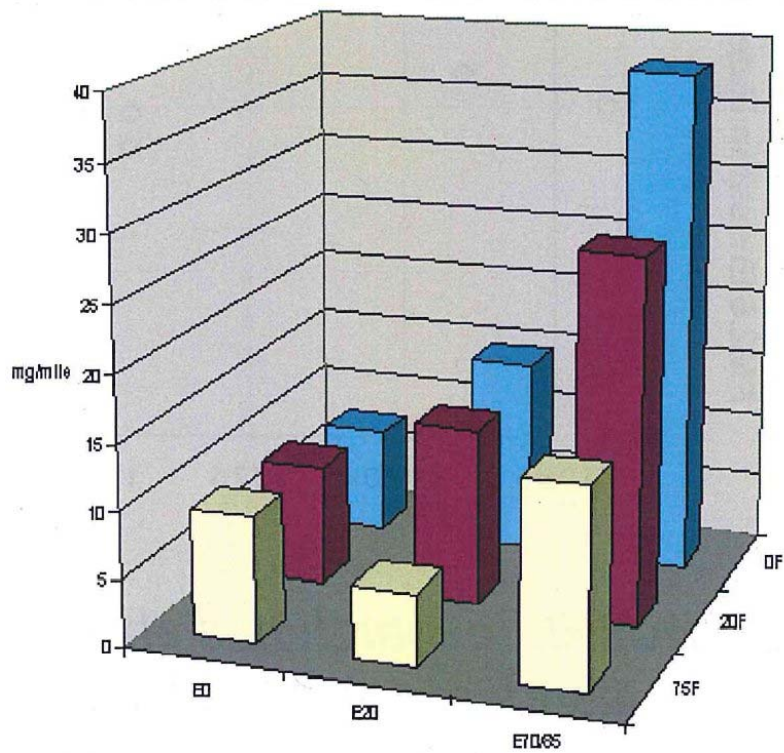


大氣溫度與交通工具粒狀物排放量關係圖

在改變汽車燃料的試驗中，發現汽車使用乙醇與汽油混合的燃料，可降低粒狀物的排放，惟卻造成乙醛排放量增加，因而產生對人體健康及空氣品質造成潛在的危害結果。



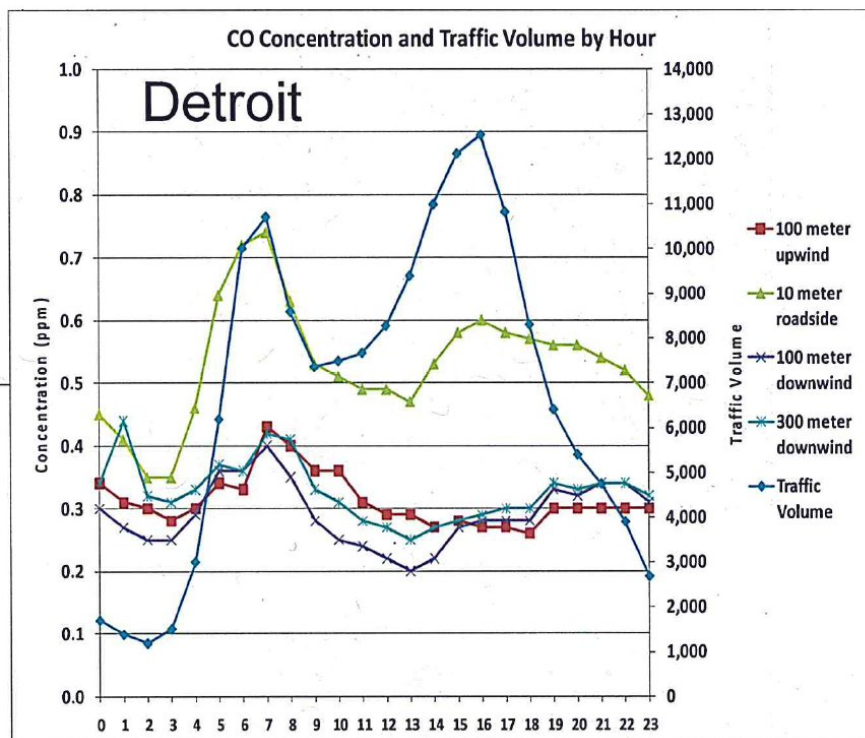
不同比例乙醇、汽油混合燃料與車輛排放粒狀物關係圖



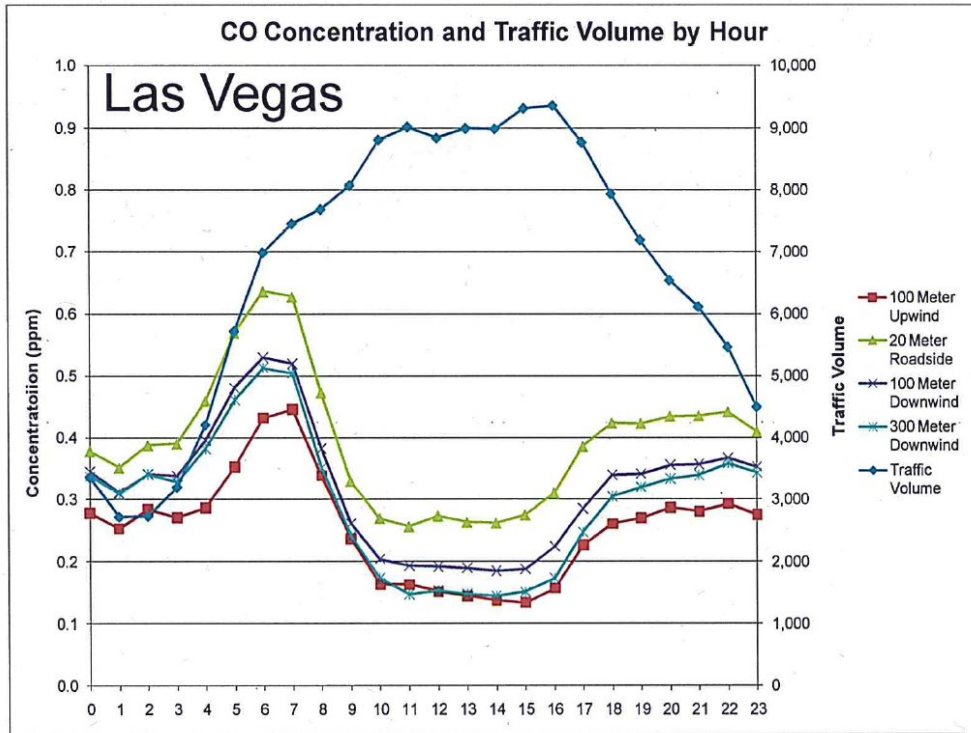
不同比例乙醇、汽油混合燃料與車輛排放乙醛關係圖

該團隊進行實地測試時，同時量測交通狀況、氣象條件及空氣品質，以固定地點採樣檢測，並使用空氣品質監測車進行移動式監測。以道路架構與現場模擬進行風洞評估試驗，並進行模式推估。

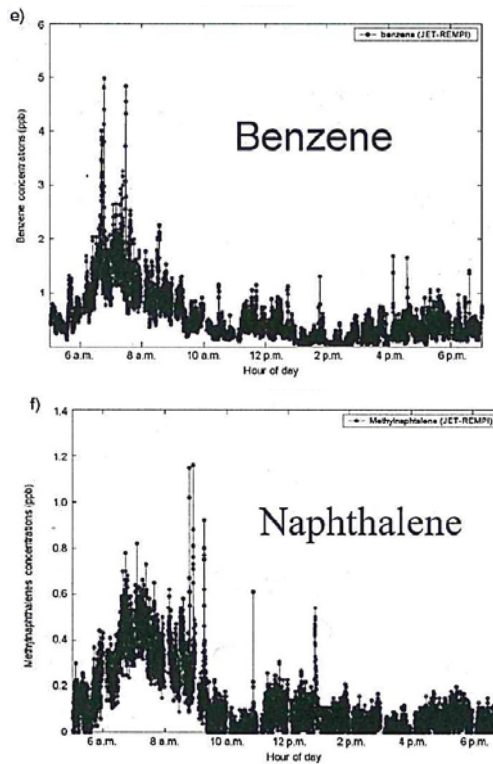
鄰近道路的空氣品質研究計畫調查結果，發現在底特律 (Detroit) 的交通尖峰時段鄰近道路的CO測值顯示最高；而在拉斯維加斯 (Las Vegas) 鄰近道路的CO測值最高時，卻不是在交通尖峰時間發生。在羅利 (Raleigh) 鄰近道路的交通工具排放污染物研究顯示，許多污染物濃度的變異，會隨著時間及空間不同而產生變化，毒性污染物 (如：苯、萘) 的濃度也隨著交通狀況、氣象條件之不同而產生變化。



底特律鄰近道路CO檢測結果 (24小時)



拉斯維加斯鄰近道路CO檢測結果（24小時）



羅利鄰近道路苯、萘檢測結果（24小時）

鄰近道路空氣品質研究計畫也評估環境、公共健康危害及學校位址設置的效益，並提供學校設址指引（School Siting Guidelines），其評估項目包括：（一）道路、鐵路、港口、機場等由交通工具排放之污染物增加而造成人體暴露的健康危害問題。（二）鄰近道路的污染物暴露危害對通勤者（路人或騎腳踏車者等）的影響。（三）學校可運用室內空氣處理（Indoor air treatment）、現場布局（Site layout）、設置屏障（Barriers）、緩衝區（Buffers）等方式，減輕遭受鄰近道路的交通排放污染。

肆、心得及建議

(一) 心得

國內對於移動污染源PM_{2.5}之檢測技術仍處技術開發階段，本次赴美國研習車輛行車型態污染排放檢測技術、黑碳檢測技術、空氣中細懸浮微粒被動採樣技術、細懸浮微粒檢測技術（SEM-EDX）、移動污染源空氣品質監測技術，並觀摩U.S. EPA RTP之PM_{2.5}分析實驗室設施及移動污染源空氣品質監測站。參訪行程中與U.S EPA RTP研究人員Richard W. Baldauf, PhD、Willis, Robert, PhD、Ronald W. Williams, PhD、Russell W. Weiner, PhD、Thomas Long、Evelyn Sue Kimbrough等人討論與交換移動污染源之檢測、監測之寶貴經驗，可提供我國發展相關移動污染源PM_{2.5}檢測技術之參考。

(二) 建議事項

- 1.目前U.S. EPA RTP使用的黑碳檢測技術，可提供國內移動污染源PM_{2.5}檢測技術研發之參考，但需注意儀器設備適用濃度的限制，以及檢測結果穩定性。建議需再進行驗證試驗，確定檢測數據符合品保、品管規定，並可應用於實際案例。
- 2.以SEM-EDX檢測PM_{2.5}被動採樣器採集之樣品，同時檢測粒狀物的巨觀形狀與微觀的元素成分，可作為污染物來源判定的分析技術，建議可提供國內發展環境污染來源鑑定技術之參考。
- 3.U.S. EPA RTP設置於I40高速公路旁的空氣品質測站，除監測空氣品質外，亦同步監測交通流量，並藉由分析空氣品質監測結果與交通流量間之關聯，可探討空氣污染事件係由交通狀況所引起，或其他因素（如：氣候）而造成。將與空氣品質相關的交通流量，同步監測、資料比對，其構想可提供國內進行環境調查、監測規劃時之參考。
- 4.U.S. EPA RTP的移動污染源空氣品質測站設有超細懸浮微粒（PM₁）檢測

設備，顯示美國環保署對於空氣中粒狀物檢測，也重視PM₁₀的相關議題。對於國內空氣中粒狀物之檢測技術發展，建議可進行PM₁₀相關之議題進行調查研究。



Transportation Emissions and Near-Source Impacts

*NRMRL Management Briefing
Oct. 24, 2012*



Office of Research and Development
National Risk Management Research Laboratory/Air Pollution Prevention and Control Division



Presentation Overview

- Background
- NRMRL Transportation-related Research
 - Motor vehicle emissions characterization
 - Near-road air quality and health effects
 - Aircraft Emissions
 - Port and rail emissions and exposures
- EPA Research Capabilities
- Example Results and Impacts

1

Background

- EPA estimates over 50 million people reside within 100 meters of a major highway, airport or rail facility
- Living, working, or going to school near major roadways has been associated with numerous adverse health endpoints
 - Respiratory effects (e.g., asthma, bronchitis)
 - Adverse birth outcomes/developmental effects
 - Premature mortality
 - Cardiovascular effects
 - Cancer
- Transportation sources are major emitters of many air pollutants
 - Criteria (CO, NO_x, Pb)
 - Air Toxics (Benzene, Formaldehyde, etc.)
 - Particulate Matter (PM_{2.5}, PM₁₀, organics, metals, etc.)



2

Background

- Understanding transportation impacts and mitigation options for protecting health and the environment require state-of-the-art, novel approaches
- NRMRL research capabilities to address these issues include:
 - Laboratory measurements of source emissions and controls
 - Field and laboratory measurements of emissions and air quality impacts
 - Laboratory analytical capabilities for sample analysis including PM and VOC speciation
 - Research and regulatory models of pollutant emissions, dispersion, and atmospheric reactions

3



Motor Vehicle Emissions

4



NRMRL Research Capabilities

- Chassis Dynamometers
 - Light-duty car and truck laboratory dynamometer
 - Temperature controlled (-20°F to 110°F)
 - Passenger cars, trucks, SUVs
 - Heavy-duty truck laboratory dynamometer
 - Portable light-duty dynamometer
 - Used all over the world
- On-board emissions measurements
 - CO, NO_x, HC, PM
 - Real-world driving
- Analytical laboratories
 - Particulate matter speciation
 - Gaseous VOC speciation



5

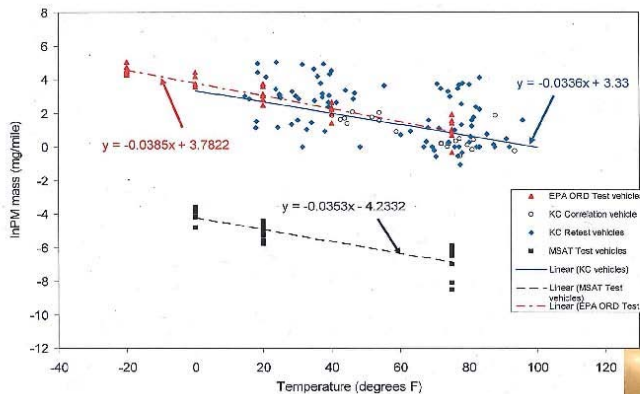
Example Projects

- Characterize emissions from transportation sources operating on alternative and renewable fuels
 - Ethanol-blend gasolines
 - Biodiesel
- Characterize and compare emissions from new technology and in-use motor vehicles
- Determine the effectiveness of emission control devices
- Determine the effect of cold ambient temperatures on vehicle emissions
- Evaluate how driving activity influences vehicle emissions

6

Collaborations with NHEERL, NERL, OTAQ, academics, industry

Ambient Temperature Effects



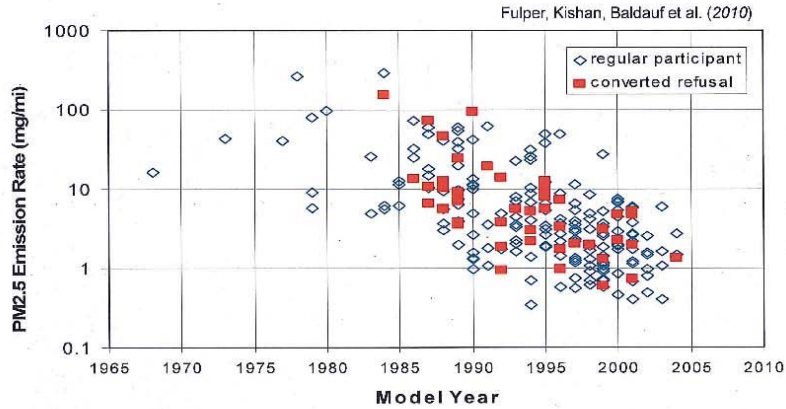
EPA's MOVES emissions model recently updated to include ambient temperature effects

NRMRL research has identified how emissions increase with decreasing ambient temperatures for varying vehicle technologies and fuels

7



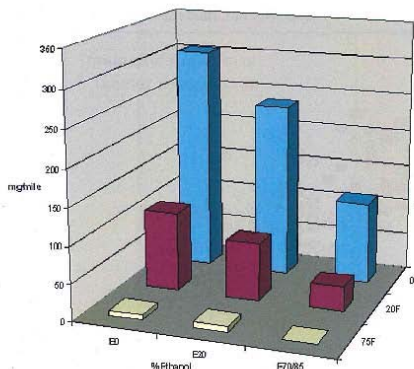
Vehicle Technology Effects



NRMRL research has shown the effectiveness of vehicle emission standards and the variability of emission rates, with a range approaching three orders of magnitude in urban fleets

8

Alternative Fuels



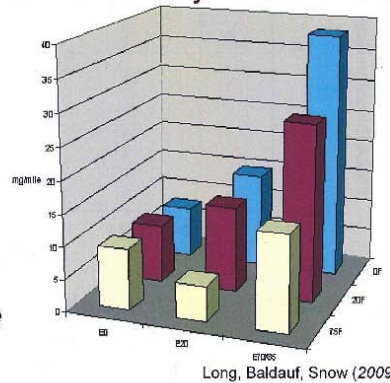
PM mass emissions

Ethanol blend gasoline can reduce PM impacts and our reliance on imported oil

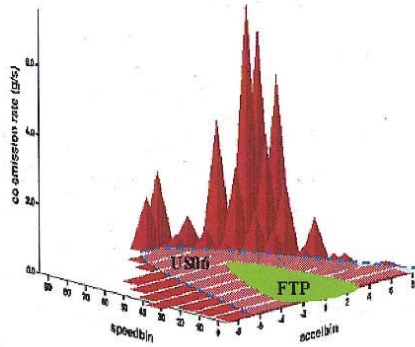
9

Ethanol blends can also increase aldehyde emissions, with potential health and air quality consequences

Acetaldehyde emissions



Driving Activity



EPA driving cycles do not capture all emissions conditions, which can dramatically increase during aggressive driving

10



Impacts of Research

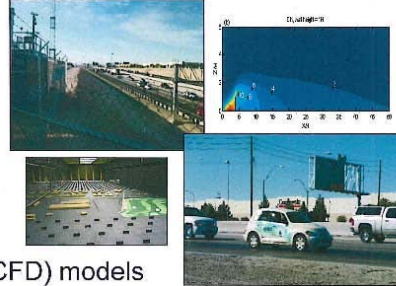
- Updated and improved the EPA's regulatory motor vehicle emissions model (MOVES)
 - Temperature effects
 - Vehicle technologies and deterioration
- Improved emission inventories for National Ambient Air Quality Standards (NAAQS), Greenhouse Gases (GHGs) and other programs
- Identified relationships among vehicle technologies, fuels, operations, and environmental conditions with air pollution emissions for regulatory and planning applications
- Determined the effectiveness of air pollution control strategies for the U.S. and Europe
- Provided data for predicting how changes in motor vehicle emissions will effect air quality, climate and health
 - E15 Waiver determination
 - Near-road impacts

11



ORD Research Capabilities

- Unique combination of field, wind tunnel and modeling
 - Field measurements of traffic, weather and air quality
 - Fixed site sampling
 - Mobile monitoring
 - Wind tunnel assessments
 - General road configurations
 - Simulations of field sites
 - Modeling assessments
 - Computational Fluid Dynamics (CFD) models
 - EPA emissions (MOVES) and dispersion (AERMOD) models



Collaboration among NRMRL, NHEERL, NERL, NCER, and OAR

13



Near-Road Air Quality

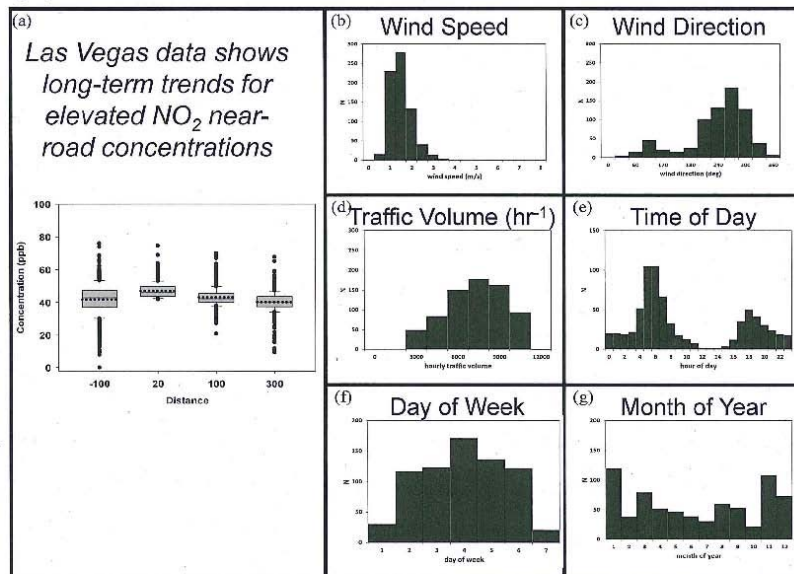
12

Research Project Examples

- Raleigh/RTP area Near-Road Studies
 - Multi-pollutant measurements
 - Toxicology comparison
 - Effects of roadside features (noise barriers/vegetation)
- FHWA/EPA collaborative studies
 - Long-term temporal and spatial measurements
 - Wind tunnel simulations
 - Modeling comparisons (MOVES and AERMOD)
- Near-Road Health Studies
 - NEXUS investigating asthma endpoints in children
 - RAMSES investigating cardiovascular effects in adults

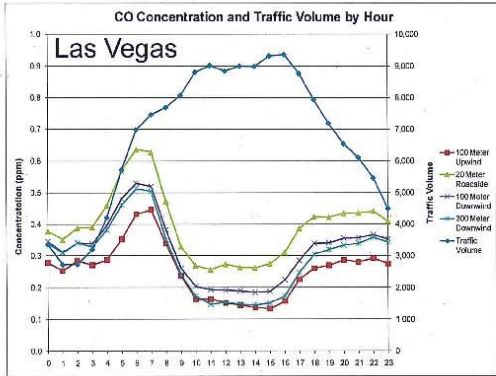
14

Traffic Emissions Impacts



15

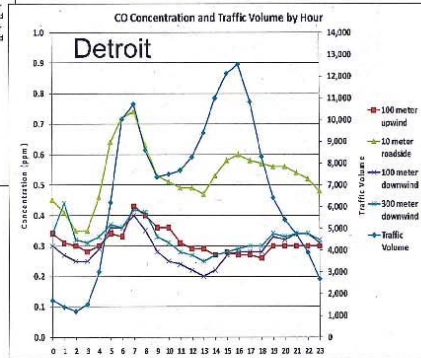
Traffic Emissions Impacts



CO measurements in Las Vegas show highest levels near the road, with elevated concentrations in the AM even without high traffic

16

CO measurements in Detroit show highest levels near the road, with concentrations elevated during rush hour traffic

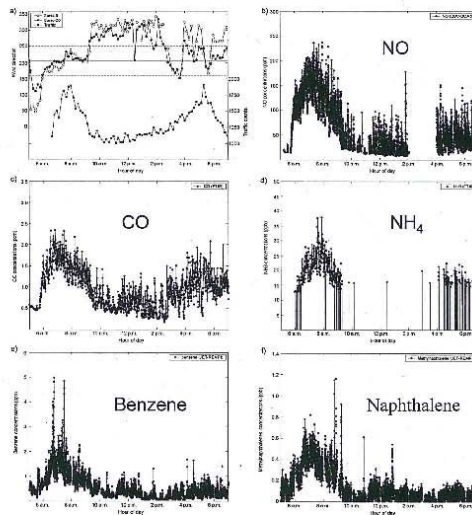


Traffic Emissions Impacts

Raleigh data shows multi-pollutant impacts, including temporal and spatial variability. Toxicity also varied with traffic and meteorological factors

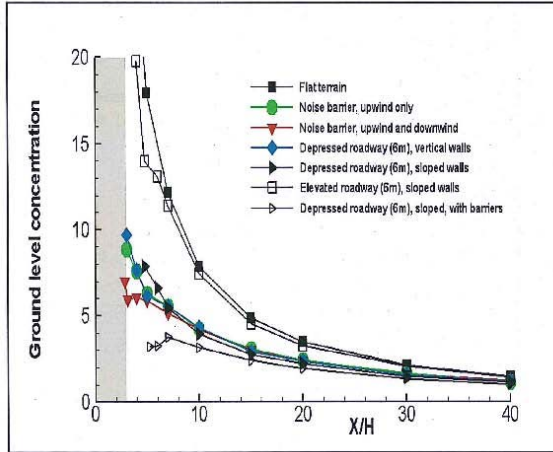
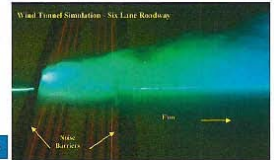


17



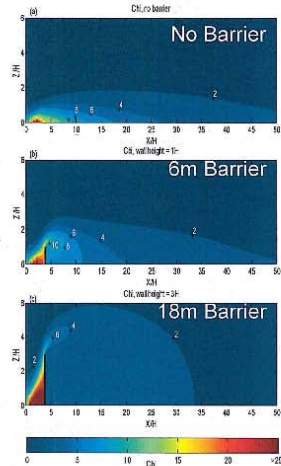
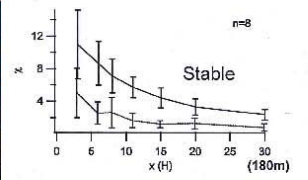
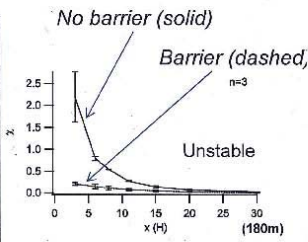
Pollutant Transport & Dispersion

Wind tunnel results show effects of changing road design and roadside features



18

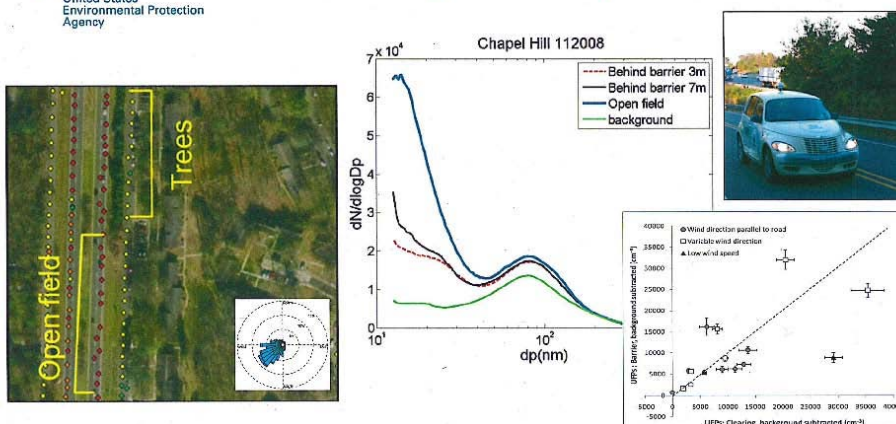
Potential Mitigation Options



Tracer studies and CFD modeling show reductions in concentrations downwind of a sound wall, although upwind, on-road levels can increase

19

Potential Mitigation Options



Vegetation may remove smaller size fractions of PM for downwind receptors; effect most evident closer to ground-level. Field study results not always consistent, variable results seen for thin tree stands and changing wind conditions (e.g. parallel to road, low winds)

20

Impacts on Scientific Understanding

- Relationships among traffic emissions and near-road air quality, population exposures and adverse health effects
- Factors influencing pollutant transport and dispersion on and from the road
- Emission and dispersion model evaluation and development
- Identifying potential mitigation options
 - Emission standards
 - Reducing vehicle activity
 - Roadside features
- Evaluating urban development practices on air quality (e.g. smart growth, multi-modal)

21

 **Impacts on EPA Programs and Policy**
United States Environmental Protection Agency

- ORD research programs in ACE and SHC
- Vehicle emission and fuel standards
 - Mobile Source Air Toxics (MSAT) rules
 - Alternative fuels assessments (E15 Waiver)
- Programs to reduce vehicle activity
 - Public transit initiatives
 - Alternative commuting programs
- Land Use and Transportation Planning
 - PM Hot Spot Conformity Guidance
 - EPA School Siting Guidelines
- NAAQS Requirements
 - NO₂ and CO Near-Road Monitoring Requirements

 **Impacts on ORD Programs**
United States Environmental Protection Agency

ACE Research Themes

Theme 1: Assess Impacts
Assess human and ecosystem exposures and effects associated with air pollutants and climate change at individual, community, regional, and global scales




ACE Tasks 013, 019, 034, 092, 180, STAR-10

SHC Tasks 1.2.5, 2.2.1, 2.2.2, 2.4, 4.1.3, 4.1.5, 4.2.1

Theme 4
Integrated Solutions for Sustainable Outcomes

The state of the practice for 4 sectors

- Materials & waste management
- Transportation alternatives
- Buildings and Infrastructure (including energy and water)
- Land Use decisions



Methods to assess Total Resource Impacts and Outcomes (TRIO) associated with community decisions – both prospectively to Inform & retrospectively to track progress

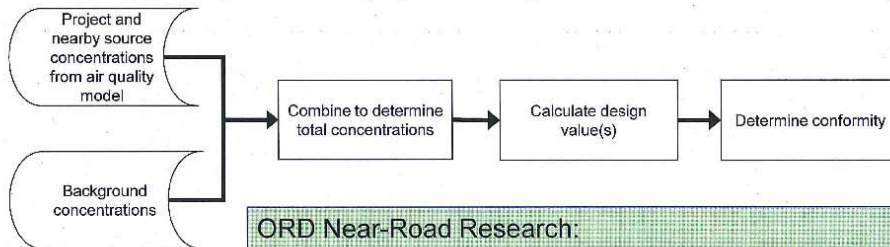
Systems models to identify options for multiple benefits

Collaborative Proof-of-Concept: Durham, NC



Transportation Conformity

- Certain projects in $PM_{2.5}$, PM_{10} , and CO nonattainment and maintenance areas required to undergo a hot spot analysis
 - Ensure a project does not cause new violations, worsen existing violations, or delay timely attainment
 - In PM areas, required for new projects with significant increases in diesel traffic



ORD Near-Road Research:

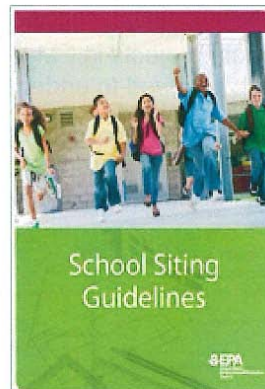
- Supported the need for the Hot Spot analyses
- Assessing models used for project assessments
- Identifying potential mitigation options for compliance

24



School Siting Guidelines

- Recommendations for evaluating the environmental and public health risks and benefits of potential school locations
- Near-Road exposures a prominent concern in the Guidelines
 - Consider health concerns from exposures to elevated pollutant concentrations from road, rail, port, airport, emissions
 - Evaluate near-road exposures with benefits of active commuting (walking, biking, etc.)
 - School mitigation options to consider:
 - Indoor air treatment
 - Site layout
 - Barriers
 - Buffers



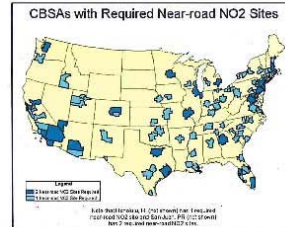
ORD Near-Road Research:

- Provided data on pollutant levels and gradients; public health concerns
- Introduced resources to assess potential hazards and risks of exposures
- Identifying potential mitigation options; design considerations and limitations



Near-Road Monitoring Requirements

- EPA now requires near-road monitoring for NAAQS attainment:
 - One near-road NO₂ monitor in each CBSA having >500,000 population
 - Second near-road NO₂ monitor in each CBSA having >2.5 million or one or more road segments with >250,000 AADT
 - One near-road CO and PM_{2.5} monitor in each CBSA with >1,000,000 population



ORD Near-Road Research:

- Provided data for NAAQS health assessments
- Justified need for multi-pollutant monitoring
- Provided foundation for guidance to states
 - Monitoring methods and implementation
 - Siting requirements and logistics



Future Activities

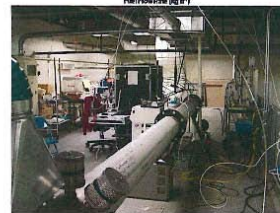
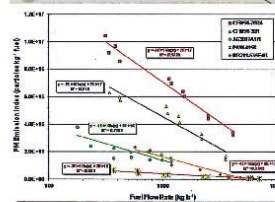
- Health Studies
 - Complete Near-Road Exposures to Urban Air Pollutants Study (NEXUS; ACE task 180 and STAR-10)
 - Begin Research Triangle Area Mobile Source Exposure Study (RAMSES; ACE task 034)
- Dispersion model evaluation and improvement (ACE task 013)
- Mitigation evaluation and quantification: Sound walls/vegetation (ACE task 092)
- Raleigh Near-Road Site/NCDENR collaboration (ACE task NEW)
- National Atlas for Sustainability improvement (SHC task 1.2.5)
- GIS-based community model development (STREET model) (SHC task 2.2.1 and 4.1.3)
- Transportation building blocks (near-road) - OSC collaboration (SHC task 4.1.3)
- Expand beyond roadways to include ports and rail (ACE task 019)

Aircraft Emissions

28

PM and Air Toxic Emissions from Commercial Aircraft Engines

- Commercial aircraft is the only non-regulated PM source in the U. S.
- A standardized method is required by EPA-OTAQ and ICAO for certification of new and in-production engines
- Extensive research has been conducted to address these needs
- Testing conducted at the engine exit, in the evolving plume, and under controlled laboratory conditions since 2004
- New instrumentation has been evaluated for the determination of black carbon emissions from aircraft engines and similar sources
- Standard test method (Aerospace Information Report) has been developed in support of OTAQ and ICAO



29

Impacts from Port & Rail Activities

30

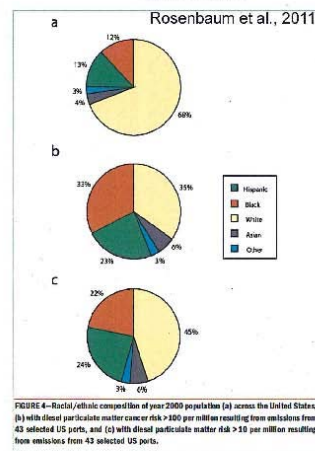
Port and Rail Research

- Urban areas have multiple transportation sources, often with concentrated emissions
- Understanding emissions is important in determining exposures and risks

Environmental Justice concerns



31



Example Research Projects

- Near-rail yard research:
 - Cicero Rail Yard Study: Region 5 RARE project CIRYS
 - Atlanta Rail Yard Study ARYS
 - Computational fluid dynamics modeling of rail yard environment CFD-RAIL

 - Near-port / multi-modal research:
 - Region 2 Port-area Investigation of Emissions Reduction: RARE project R2PIER
 - PANama Canal expansion and Air Quality study PANCAQ
- ...utilizing a combination of modeling, field measurement, and GIS analyses

32

Cicero Rail Yard Study

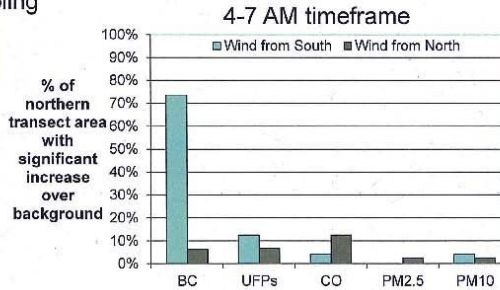
- Cicero Rail Yard is located in densely populated suburb of Chicago
- Intermodal rail yard; emission sources include: trucks, cranes, switcher locomotives, trains passing through (commuter and freight) and idling.
- Estimated container lift volume: 400,000; other Chicago-area intermodal hubs ranging ~100,000-800,000



33

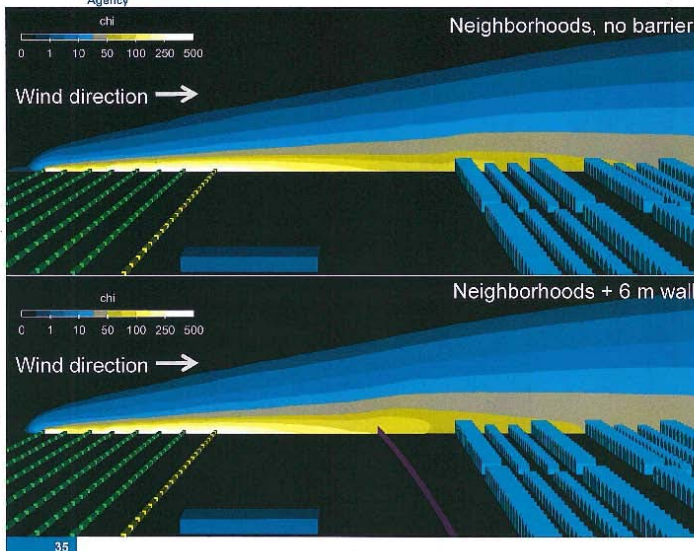
Cicero Rail Yard Study

Example findings from mobile sampling



For 3 early morning sessions with wind from S: "...excess concentration of 0.3-0.6 $\mu\text{g m}^{-3}$ BC, 30-40% higher total BC concentrations relative to the urban background (background ranged 0.8-2.0 $\mu\text{g m}^{-3}$ BC). The other measurements shown – UFPs, CO, PM_{2.5} and PM₁₀ – do not show the same upwind/downwind trend of excess levels"

Rail Yard CFD modeling



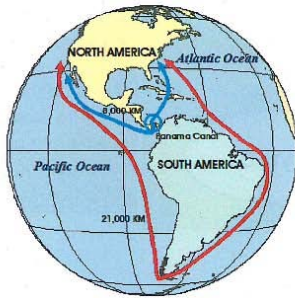
CFD modeling being used to evaluate measurements, determine neighborhood concentrations and exposures, and consider effectiveness of a boundary wall for mitigation



Panama Canal Expansion

“By 2020, even at moderate rates of economic growth, total domestic tonnage of freight carried by U.S. freight systems will increase by 100% in the West, 89% in the Midwest and South, and 79% in the Northeast. In this same timeframe, every major U.S. container port is expected to at least double in volume, with select East Coast ports tripling their volume and some West Coast ports quadrupling.”

Source: U.S. Maritime Administration, 2009



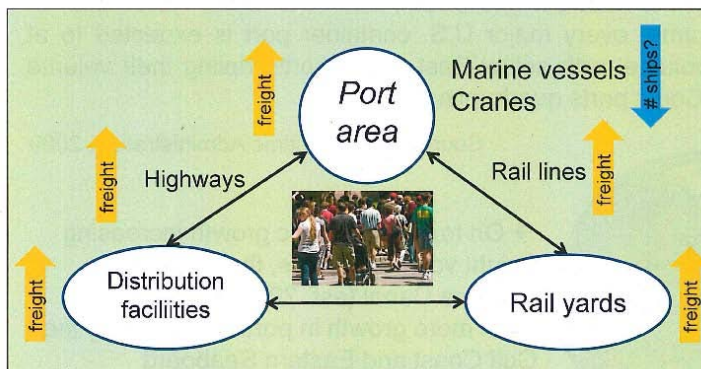
→ On top of economic growth increasing freight volume at ports, the expanded Panama Canal (est. 2014) may lead to even more growth in port activity along the Gulf Coast and Eastern Seaboard

36



Port Research – near-source air quality

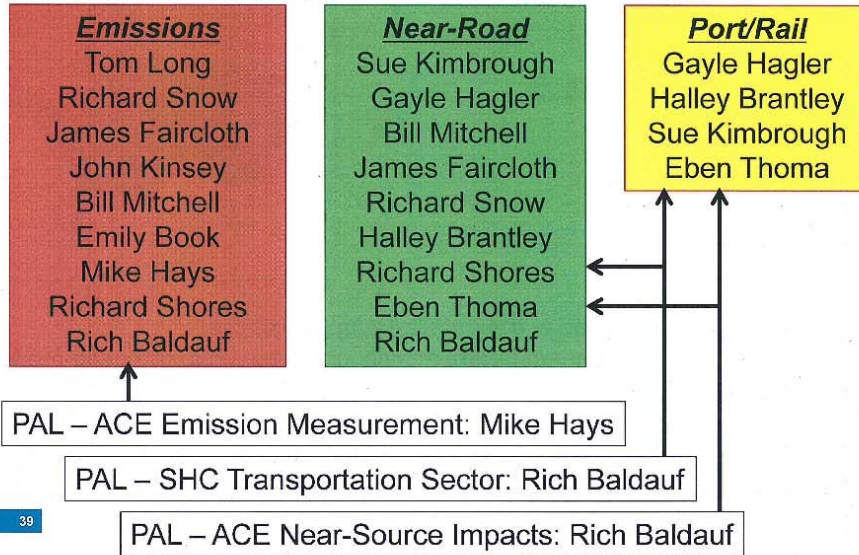
Concept of linked emissions; location of source and population key for near-source impact



Factors:
- New standards lowering emissions
- Voluntary measures to lower emissions
- Larger Post-Panamax ships may replace several smaller ships
- Overall increase in freight anticipated

37

NRMRL Research Team



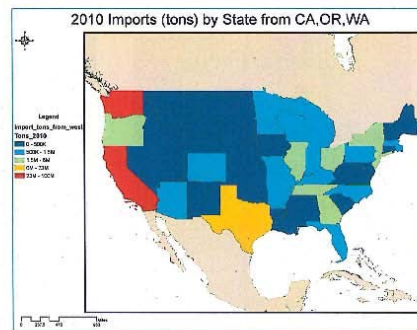
39

Port Research

Understanding baseline conditions:

5 Ports selected for analysis:

- Port of NY/NJ
- Port of Savannah
- Port of Norfolk
- Port of Houston
- Port of Miami



Questions being addressed in the detailed analysis phase:

- + How closely can we connect freight activity changes along the multi-modal transportation network?
- + What are the population demographics in the near-source areas (50, 100, 300 m) along the freight distribution network for a particular port?
- + What is the existing air quality status (criteria pollutants and air toxics)?

38



Partners/Collaborators

EPA Program Offices

Office of Transportation & Air Quality (OTAQ)
Office of Air Quality Planning & Standards (OAQPS)
Office of Sustainable Communities (OSC)
Office of Children's Health Protection (OCHP)
Regions (notably 2,4,5,6,9)

State & Local Agencies

California Air Resources Board
Georgia Env. Prot. Div.
N. Carolina Dept. Env. & Nat. Res.
Clark County Air District
Atlanta Regional Comm.
Michigan DEQ/Michigan DOT
Texas DOT
Florida DOT

Professional Org.

Coord. Research Council
Transp. Research Board
AASHTO
American Public Health Assoc.

NRMRL Transportation Research

Federal Agencies

U.S. Dept of Transportation
Fed. Highway Administration
Federal Transit Agency
Centers for Disease Control
U.S. Dept. of Energy
U.S. Forest Service

Academic Inst.

Univ. North Carolina
N. Carolina State Univ.
Duke Univ.
N. Carolina Central Univ.
Cornell Univ.
Univ. Michigan
Univ. Cincinnati
Univ. California-Davis
Univ. California-Berkeley
USC/UCLA

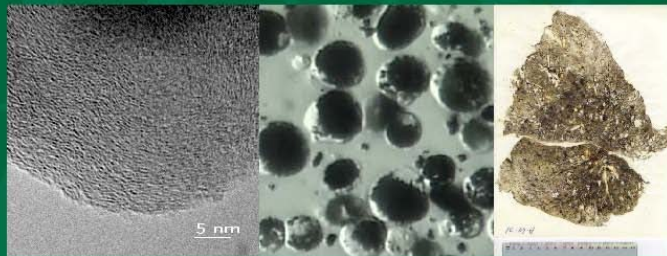
International

European Union Comm.
World Health Org.
Japan Auto Manuf. Assoc.
China Ministry Sci. & Tech.

40

BC measurement activities at the US EPA (ORD-RTP)

Michael D. Hays



Office of Research and Development
National Health and Environmental Effects Research Laboratory and National Risk Management Research Laboratory

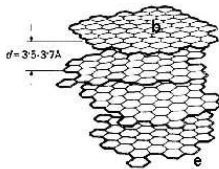
June 18, 2012

Carbon classification by analytical method

	Thermochemical Classification	Molecular Structure	Optical Classification
↑ Refractiveness	Elemental Carbon (EC)	<i>Graphene Layers (graphitic or turbostratic)</i>	Black Carbon (BC)
	Refractory Organics	<i>Polycyclic Aromatics, Humic-Like Substances, Biopolymers, etc.</i>	Colored Organics
	Non-Refractory Organics (OC)	<i>Low-MW Hydrocarbons and Derivatives (carboxylic acids, etc.)</i>	Colorless Organics (OC)
			↑ Specific Absorption

different sources emit these in different proportions

Black carbon generation



- BC forms in fuel-rich, poorly mixed hot (1600 °K+) flames
- from fuel-nascent PAH; H abstraction; or other mechanisms (C5)
- other factors include flame residence time, metal catalysis etc.

- proportion of b/e can effect adsorption, soot reactivity, wettability
- soot is oxygenated; not graphite per se

4

with help from Bond tutorial

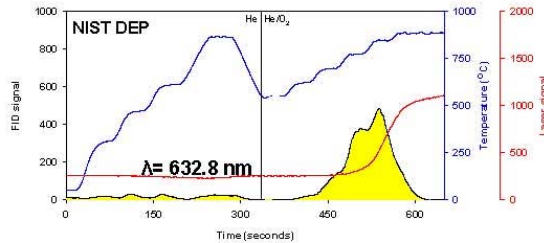
(Ground-based) Carbon measurement techniques

- current techniques
 - thermal-chemical or “evolved gas” analysis
 - thermal-optical analysis
 - NIOSH, 5040, EPA-NIST, and IMPROVE
 - light absorption measurements
 - filter-based – aethalometer, PSAP, MAAP [scattering correction]
 - direct on the aerosol – photoacoustics, incandescence (SP2)
 - Raman spectroscopy
 - molecular level, functional group concentration
 - poor for routine monitoring
 - HR-TEM
 - qualitative
- possible future techniques
 - high-resolution MS
 - chemical formulas
 - not always a matter of defining specific chemical structure
 - spectral absorption
 - fluorescence lidar
 - remote sensing technique
 - photophoretics
 - XPS

5

Thermal and thermal-optical techniques

- semi-continuous (30 min, 0.5 $\mu\text{g}/\text{m}^3$) or integrated samples (0.2 $\mu\text{g}/\text{cm}^2$) {field and lab}
- multitude of thermal programs, reflectance, transmittance
- ambient monitoring networks rely on these methods

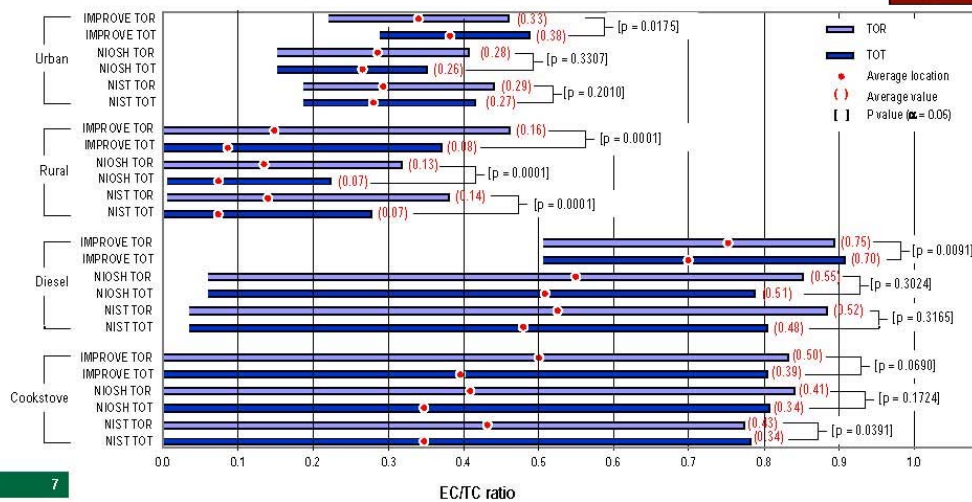


- thermal technique issues (French method)
 - filter-sample interactions and oxidant composition varies
 - charring (possibly avoided with extractions, more temp. steps = tedious)
- thermal-optical techniques correct for charring but...
 - carbon with OC- and EC-like properties ("brown carbon" [likely invisible])
 - EC not a proxy for LAC
 - light extinction of char varies with that of native BC
 - methods disagree for some sources (in-filter charring)

6

widely used; EPA

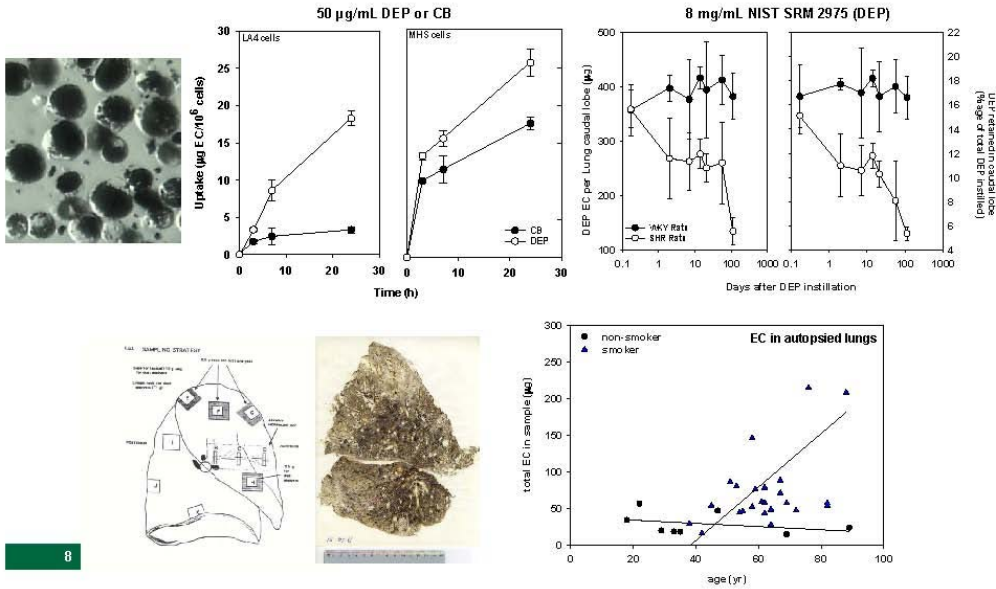
Differences in the OC/EC Ratios that Characterize Ambient and Source Aerosols due to Thermal-Optical Analysis Bernine Khan, Michael D. Hays, Chris Geron & James Jetter (2012, 46: 127-137)



7

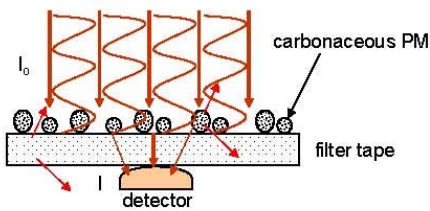
Thermal-optical transmittance for EC in biological samples

Saxena et. al., *Tox. Sci.* 111(2), p. 392 (2009); and *Biotechniques* 44, p. 799 (2008)

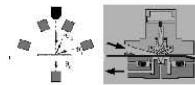


8

Light absorption techniques (filter-based)



- Aethalometer
- Particle Soot Absorption Photometer (PSAP)
- Multi-Angle Absorption Photometer (MAAP)
- Difference method (loading issue)



Petzold et al. 2005

- on-line, semi-continuous methods
- $A = \ln(I_0/I)$ proportional $\alpha_{abs} C$
 - $\alpha_{ATN} = \alpha_{ABS} / C_{soot} = 1-30 \text{ m}^2/\text{g}$
- dual or multiple wavelengths

limits

- lack of reference standards
- no unique α_{abs} for conversion
- PM aging
- filter-aerosol interactions
 - scattering
 - shadowing
- systematic errors up to 2

Technique	λ (nm)	BC Sensitivity*	operation
Aethalometer	370, 470, 520, 590, 660, 880 (ir), 950	100 ng/m ³ at 1 min	transmission
PSAP	567	—	transmission, ref. filter, loading
MAAP	670	100-20 ng/m ³ at 2-30 min avg	sim. multi-angle, transmission, reflectance

*depends on spot size

9

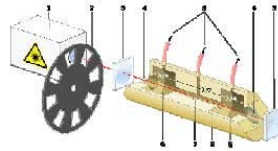
α – mass-specific absorption coefficient

widely used; EPA

Light absorption techniques (direct)

Photoacoustics spectrometry (PAS)

- continuous, suspended state
- absorbed energy → acoustic pressure wave
- no response to light scattering
- issues
 - drifting
 - expensive
 - used less
 - cross-sensitive to NO_x



$$b_{\text{PAS}} = Pm \pi 2A_{\text{res}} f_0 / PLQ (\gamma - 1) = \alpha_{\text{ABS}} \cdot C_{\text{soot}}$$

cell cross sectional area, resonator quality, laser power
carrier gas specific heats

Droplet Measurements Technology [DR1]

- PASS-1 and -3
- one or three λ settings
- 50 ng/m^3 @ 1 sec integration

AVL [TUM] (source emissions)

- $\lambda = 808 \text{ nm}$
- 5 $\mu\text{g}/\text{m}^3$ (up to 50 mg/m^3)

10

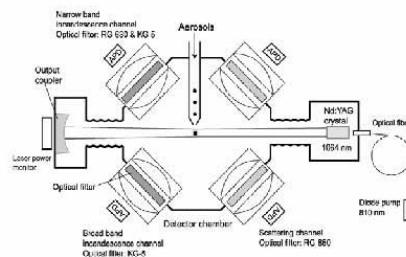
BECOMING widely used

Laser-induced incandescence (LII)

- in-house designs
 - combustion and flame experiments
- not routine

Example: PS2 (Droplet Measurement Technologies)

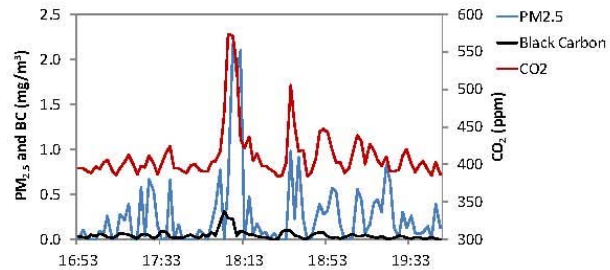
- real-time single particle technique
 - sub-femtogram ($d_a = 70 \text{ nm}$)
- 4 optical axis measure scattering and LII emissions
 - non-absorbers sized ($d = 250\text{-}1000 \text{ nm}$)
 - heated (1000 K) to incandesce – vaporize organics
 - sensitive to soot f_v
 - image output
 - LII peak can be used for BC particle sizing
 - $d_a = 50\text{-}500 \text{ nm}$ (mass equivalent diameter)
- issues
 - relatively new (can be linked to AMS)
 - expensive
 - max no. conc = 5000 particles/ cm^3



11

less widely used

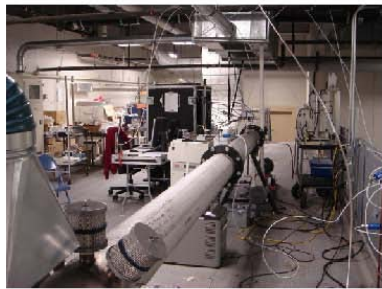
Aerostat sampling of PM_{2.5}, BC, and CO₂ from prescribed forest fire – Eglin Air Force Base, FL (Brian Gullett)



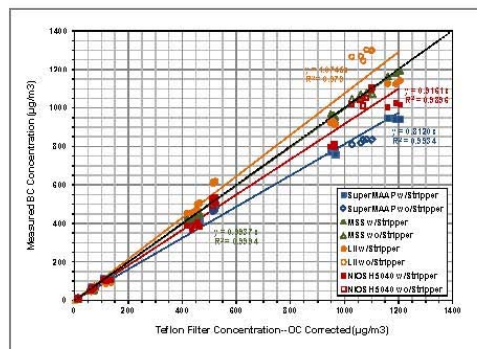
- 200-300 ft aloft
- vertical plume distribution
- 2-min average.
- ambient air CO₂ concentration: 390 ppm

12

Characterizing PM emissions from commercial aircraft engines (John Kinsey)



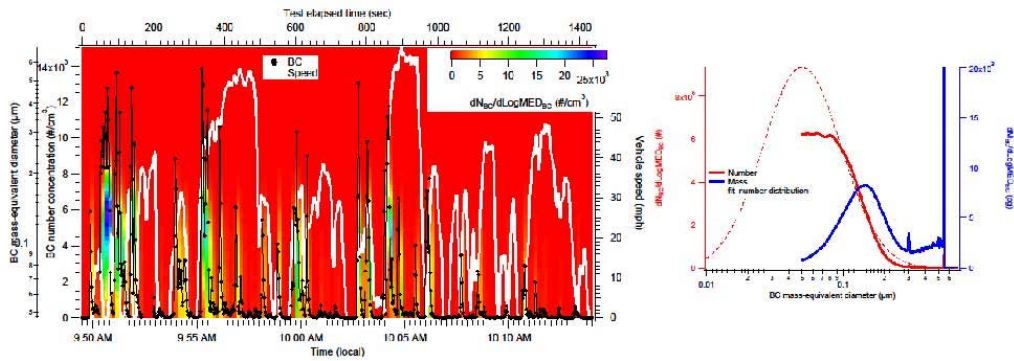
Lab-scale flow tunnel system used for BC instrument evaluation.



Can a standardized test method be developed for measuring non-volatile PM emissions for use in aircraft engine certification world-wide?

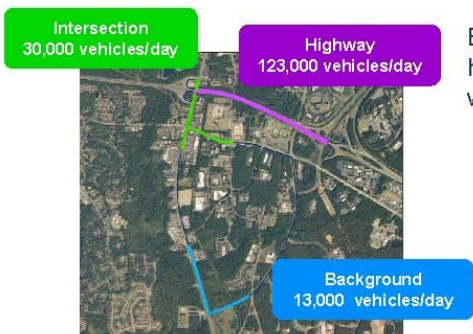
13



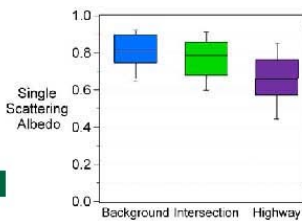
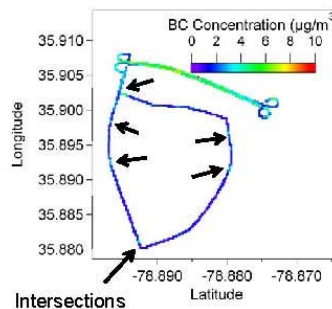


14

Done with DMT (Subu)



Black carbon concentrations are highest on the highway, but are also elevated at intersections where vehicles accelerate from a stop.



Similarly, particle optical properties vary by location. Strongly absorbing particles dominate on the highway leading to low SSA values.

15

Done with DMT (Subu)

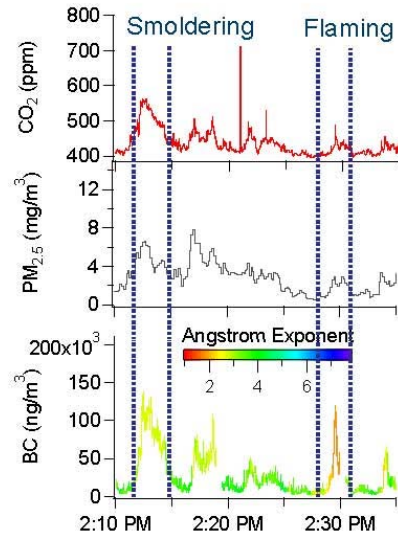
Ground level particle emissions from a prescribed fire at Ft. Jackson, SC – Amara Holder

Samples from the fire plume are identified by the CO₂ concentration and the combustion regime is identified by the angstrom exponent (α).

Flaming
α ~ 1

$$B_{abs} = \lambda^{-\alpha}$$

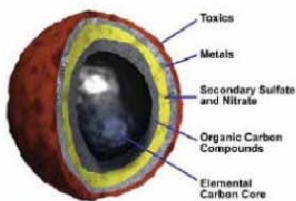
Smoldering
α > 1



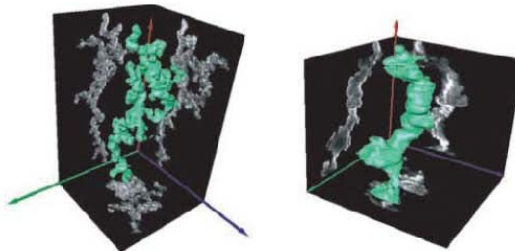
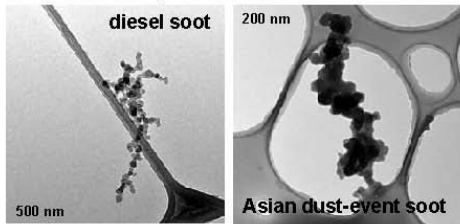
16

Visualizing soot

classic particle model



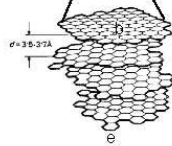
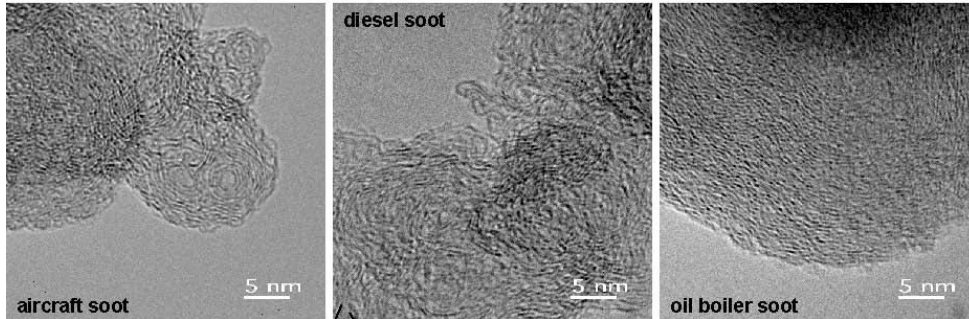
Electron tomography with TEM images
Adachi et al. 2007, JGR



improved D_r, R_g, A_v/V, k_a

17

Visualizing black carbon



- BC is nanoheterogeneous
- internal and external mixture
- interior-perimeter effects
- fullerenic structure – anthropogenic emissions
- fringe analysis confirmed subtle differences
- variety of soot types in atmospheric aerosols

18

with help from Bond tutorial

Experimental setup

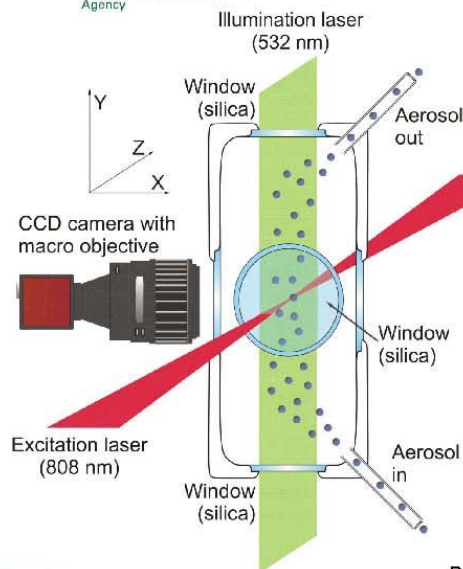
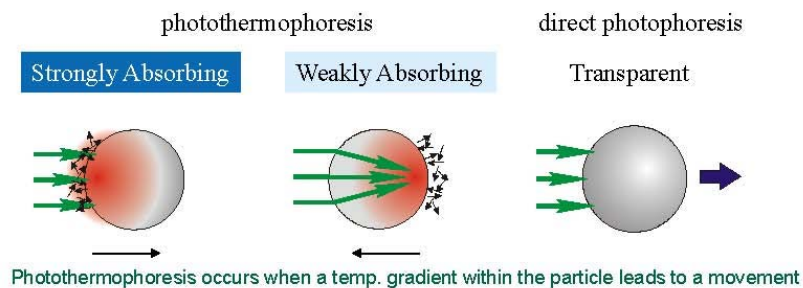


Photo of the Setup
(phototonics spectra 4/2008)

Profile of the illumination laser is modified to a thin layer to observe only the by the excitation laser affected particles

19



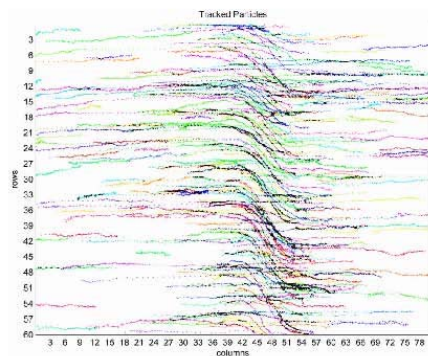
20

Photophoretic Velocimetry for the Characterization of Aerosols

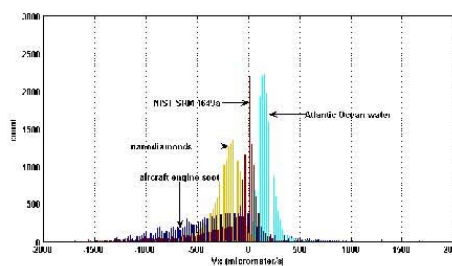
Christoph Haisch, Carsten Kykal, and Reinhard Niessner
Analytical Chemistry **2008** 80 (5), 1546-1551

in development at TUM

Results



tracking results (single experiment)



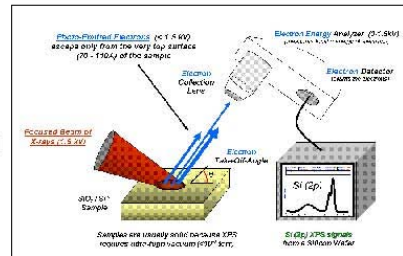
21

Photo-thermophoresis as a new tool for aerosol characterization.

Haisch, C., Opilik, L., Hays, M., and Niessner, R.. (2009) *Journal of Physics: Conference Series*, in review.

XPS technique and experimental details

- measured difference between ejected electron energy and incident beam = binding energy
- 1-10 nm sample depth
- survey scan and high resolution scan
 - elements determined to within $\pm 0.1\%$ (atomic)
 - HR scan for carbon bonding states and functional groups (10 sweeps 7 cycles)
 - curve fit C1s binding region
 - Lorentzian and Shirley fit

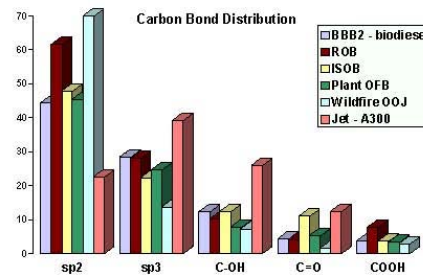
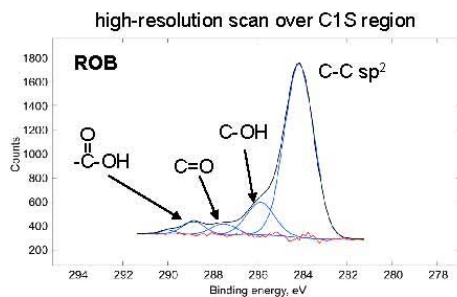


- examined emissions from plant-, institutional-, and residential-scale oil boilers, diesel and bio-diesel engine exhaust, wildfire, and aircraft engines

22

rarely used

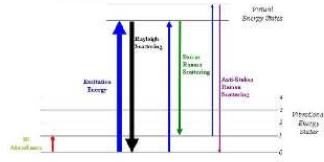
XPS (ESCA) for aerosol surface chemistry



- percentages of carbon atoms apportioned to oxygen functional groups
- slight shift in C1s binding energy indicate different oxygen functional groups
- different carbon bonding states at the particle surface

23

Raman spectroscopy

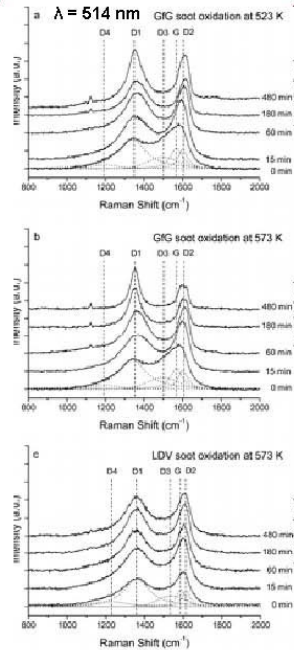


- specific to vibrational and rotational modes
- sensitive to electron clouds and bonds
- ground state >>> vibrational energy state
- chemical structure and soot reactivity

- defect (D) and graphite (G) peaks
 - G – ideal graphite
 - D1 – vibration mode graphene e
 - D2 – vibration surface graphene
 - D3 – amorphous, organics
 - D4 – disordered graphite and sp³

24 Ivleva et al. EST 2007

with help from Wikipedia



rarely used

Upcoming BC Investigation: Stationary Diesel Generators

• Three different generators will be tested with and without after-market, post-combustion emissions controls for emissions factors

- ~300hp, 500hp, and 700hp diesel generators
- Post-combustion controls will vary but will fall within the categories of:
 - Active DPF
 - Ceramic
 - Oxidative catalyst

• Instrumentation/Methodology to be used:

- Aethlometer
- Photoacoustic
- LII
- Thermal-optical (NIOSH5040 or IMPROVE)
- CEM benches to monitor combustion gases
- PM mass via teflon filter collection



After-market active DPF installed on diesel generator (photo courtesy of Rypos)



Refine thinking to climate-relevant properties of PM

- likely interlaced with metals and organic matter over a strongly adsorbing matrix
 - i.e., BC is not alone
- organic matter on PM is light absorbing
 - nitrated and aromatic aerosols
- uneven surface coverage of chemical groups
 - very poor knowledge of surface chemistry in general
- atomic order gives rise to nano- and micro-structure which changes conformation and binding properties of soot
- photophoretics suggests physical and chemical properties impacts optical properties

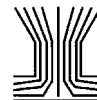
26



Conclusions

- Selection of BC instrument depend on aerosol sample being taken and information needed
- Instruments can be designed, modified, and outfitted to solve specific problems
- Advancements are being made
 - Newer instrumentation will be available
- Source aerosol emissions are studied relatively less than atmospheric aerosols

27



Passive Aerosol Sampler. Part I: Principle of Operation

Jeff Wagner and David Leith

*University of North Carolina, Department of Environmental Sciences and Engineering,
Chapel Hill, North Carolina*

A method has been developed to estimate average concentrations and size distributions with a miniature passive aerosol sampler. To use the passive sampler, one exposes it to an environment for a period of hours to weeks. The passive sampler is intended to monitor ambient, indoor, or occupational aerosols and has potential utility as a personal sampler. The sampler is inexpensive and easy to operate and is capable of taking long-term samples to investigate chronic exposures. After sampling, the passive sampler is covered and brought to the lab. Scanning electron microscopy (SEM) and automated image analysis are used to count and size collected particles with $d_p > 0.1 \mu\text{m}$. Alternatively, more advanced microscopy techniques can be used for ambient-pressure analysis or elemental characterization. Image analysis is used in conjunction with particle density and shape factors to obtain the mass flux as a function of aerodynamic diameter. The flux and a deposition velocity model are then used to estimate the average mass concentration and size distribution over the sampling period. The deposition velocity model consists of a theoretical component and an empirical component. The theoretical component incorporates gravitational, inertial, and diffusive mechanisms, but can be approximated by the simple terminal settling velocity in many cases. This article, Part I, describes how measurements are made with the passive sampler. The sampler design, theoretical component of the deposition velocity model, and microscopy methods are presented. Part II describes wind tunnel experiments performed to measure sampler precision and determine the empirical component of the deposition velocity.

INTRODUCTION

Epidemiological studies have shown a relationship between particle exposure and community health effects (e.g., Dockery et al. 1993; Thurston et al. 1994; Pope et al. 1995). The causal mechanisms in this relationship are not yet clear, partly due to uncertainties in exposure assessment. In occupational and indoor environments, the threat posed by specific aerosol toxins is better understood, but many aerosol exposures remain uncharacterized.

Received 13 April 1999; accepted 10 December 1999.

Address correspondence to Jeff Wagner, University of North Carolina, Department of Environmental Sciences and Engineering, CB#7400, Rosenau Hall, Chapel Hill, NC 27599. E-mail: jrwwagner@lbl.gov

Current techniques to assess aerosol exposures have limitations. For example, long-term chronic exposures are often estimated by averaging several short-term samples. Obtaining a reliable average with this approach is difficult, however, because short-term levels may vary over time or be autocorrelated (Rappaport 1994). Mean exposure can also be assessed with a continuous monitor, but power and maintenance requirements make this method relatively expensive.

Another problem is the large number of samplers needed for some types of exposure studies. Monitoring community exposure with a few centrally-located samplers may not adequately represent exposures in outlying regions (Liu et al. 1995). Similarly, multiple samplers are required to represent the exposure variability between individuals in heterogeneous populations. Many samplers are also needed to investigate the relationship between indoor, outdoor, and total personal exposure levels (Suh et al. 1992). These tasks can be costly and labor intensive if conventional pump-operated samplers are used.

Although personal samplers are typically much smaller than stationary samplers, their sampling pumps can be noisy, heavy, or bulky. This issue is important because any inconvenience experienced by a person wearing a personal sampler may alter behavior and produce nonrepresentative exposure estimates (Wiener and Rodes 1993).

This paper presents a miniature passive aerosol sampler that can be used to estimate long-term average size distributions and concentrations. The passive sampler is intended to monitor ambient, indoor, or occupational aerosols over a period of hours to weeks and has the potential to be used as an area monitor or as a personal sampler. The longer sampling times of the passive sampler should improve assessments of long-term mean exposures. The sampler is cheaper and easier to operate than conventional samplers and therefore a larger number of passive samplers can be deployed. Because the passive sampler is much lighter, smaller, and quieter than pump-operated personal samplers, it may yield more representative measurements.

During sampling, particles passively deposit on the sampler's collection surface. Afterwards, the sampler is enclosed in a plastic case and transported to the lab for analysis using scanning electron microscopy (SEM). Alternatively, more advanced

microscopy techniques can be used for ambient-pressure analysis or elemental characterization. During SEM analysis, collected particles with $d_p > 0.1 \mu\text{m}$ are representatively counted and sized and elemental compositions can be determined as well. The resulting flux measurement (particles collected/(area-time)) and a semiempirical deposition velocity model are then used to determine the average concentration and size distribution to which the sampler was exposed.

Previous investigators have raised concerns about passive sample collection, noting that particle deposition is dependent on wind speed and particle size (Lehtimaki and Willeke 1993). Indeed, simply examining the deposited particles without considering the physics of the particle deposition will lead to highly uncertain and distorted size distribution calculations. For this reason, the present work incorporates a deposition velocity model that calculates particle deposition as a function of both particle size and turbulence level.

The passive sampler developed in this research differs from the designs of previous investigators in several respects. The passive dust monitor of Brown et al. (1995) collects particles electrostatically with a charged electret. Calculation of aerosol concentration requires knowledge of the average aerosol electrical mobility and electret charge. Alternatively, electret mass can be correlated with the results of conventional samplers (Brown et al. 1996). The passive sampler of Vinzents (1996) collects particles onto upward-facing, sideways-facing, and downward-facing substrates. A light extinction technique can be used to provide an index of mass concentration. The sampler of Vinzents measures approximately $14 \text{ cm} \times 6 \text{ cm} \times 5 \text{ cm}$, somewhat larger and heavier than the passive sampler of this research.

This article begins with a brief description of the sampler design. The sampling and analysis procedures for the passive

sampler are then described, including the theoretical basis of the deposition velocity model and the microscopy methods. Part II describes tests conducted on the passive sampler using a specially-designed wind tunnel (Wagner and Leith 2001).

SAMPLER DESIGN

The design objectives for this research were to create a passive sampler that is small and lightweight, sturdy, convenient for microscopy analysis, and resistant to sample contamination or resuspension. A schematic of the passive sampler is shown in Figure 1. The body of the sampler is composed of either an aluminum or carbon SEM sample mount. Aluminum-based samplers are preferable for size distribution analyses because their high conductivity allows for good resolution. Carbon-based samplers are preferable when elemental analysis is important to minimize interference with the elemental spectra. A 1.5 cm diameter cap supporting a stainless steel mesh is mounted onto the SEM base with spray mount adhesive. The spray mount securely fastens the mesh caps during sampling, but allows removal of the caps afterwards for analysis. The semiquiescent collection region is 1.2 mm deep and 6.8 mm in diameter, and the mesh is $127 \mu\text{m}$ thick. Because the machining of the SEM substrates often creates microscopic grooves and imperfections, a circular collection surface of smooth aluminum tape is mounted on the "floor" of the collection region. The particles that collect on the smooth substrate can then be analyzed with a minimum of interference.

The purpose of the mesh cover is to prevent deposition of very large particles, such as sand, hair, or other debris, onto the collection surface. The particle sizes that are removed by the mesh are determined by the mesh pore size. A smaller mesh size

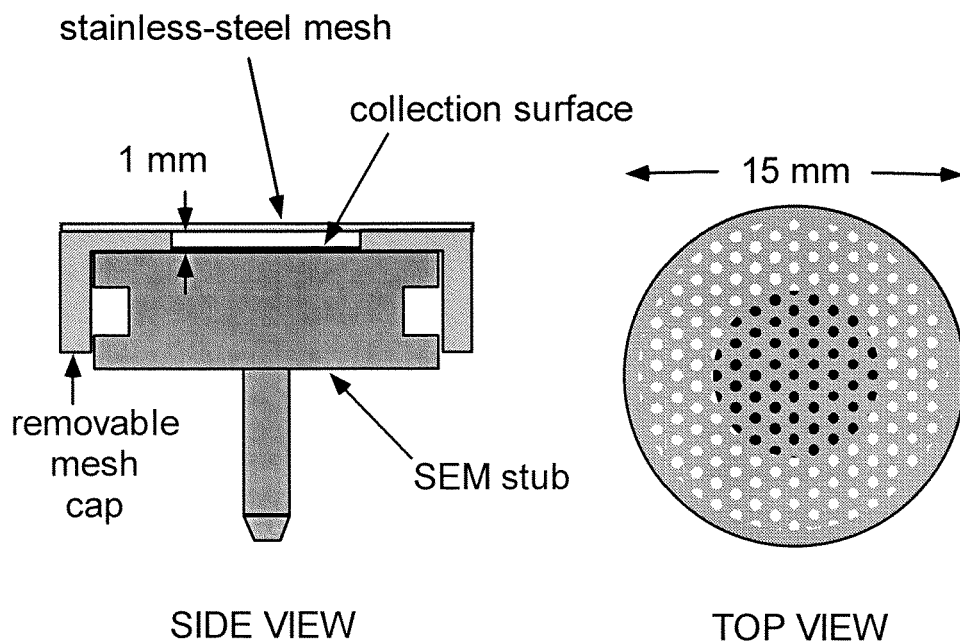


Figure 1. Passive sampler design.

is desirable because it will prevent more unwanted large particles from depositing. However, a smaller mesh size will also collect some smaller particles by diffusion and interception, which will reduce the total sample size. Thus the mesh size was selected to reach a compromise between these two concerns. A mesh with holes of conical cross section and dimensions of $160\ \mu\text{m}$ (top diameter) and $225\ \mu\text{m}$ (bottom diameter) has been selected for general use (Buckbee-Mears, St. Paul, Inc.). However, a range of mesh sizes is commercially available and can be selected with respect to the sampling application.

DEPOSITION VELOCITY MODEL

Several particle deposition models have been described in the literature for various applications, including studies of atmospheric dry deposition, particle deposition in microelectronic clean rooms, smog chamber wall losses, and indoor air deposition (e.g., Sehmel and Hodgson 1978; Slinn and Slinn 1980; Liu and Ahn 1987; Nazaroff and Cass 1987; Cooper et al. 1989; Schneider et al. 1994). An expression commonly used in these models is the deposition velocity:

$$v_{dep} = F/C, \quad [1]$$

where F is the flux of particles to a given surface and C is the bulk aerosol concentration. The deposition velocity, F , and C are all functions of particle diameter.

These models vary in the particle transport mechanisms they consider. For this research, the relevant deposition mechanisms are convective diffusion, inertia, and gravitational settling. Thermophoresis, electrostatic Coulomb forces, and electrostatic image forces have not been included in the model. Any temperature gradients that occur between the sampler surface and the surrounding air are expected to be random and short lived. Therefore the average temperature gradient is assumed to be zero over the several-week sampling period. Similarly, any voltages that accumulate on the sampler are expected to be transient rather than continuous and would be difficult to quantify accurately. Nevertheless, when possible the sampler should be grounded. The magnitude of electrostatic image forces are probably not important compared to the other deposition mechanisms (McMurry and Rader 1985).

A schematic for the deposition velocity model is shown in Figure 2. A collected particle is assumed to travel from the turbulent atmosphere into the passive sampler's boundary layer, through the sampler's mesh holes, into the sampler's collection region, and finally onto the collection surface. Along this path, several factors specific to the sampler and mesh geometry can affect particles' deposition velocities. For one, if the surrounding wind currents have a large horizontal component, particles can be removed on the leading edge of the sampler by inertia, diffusion and interception. In addition, some particles will be removed by the mesh as they pass into the collection region. Even those particles that travel into the mesh holes can be

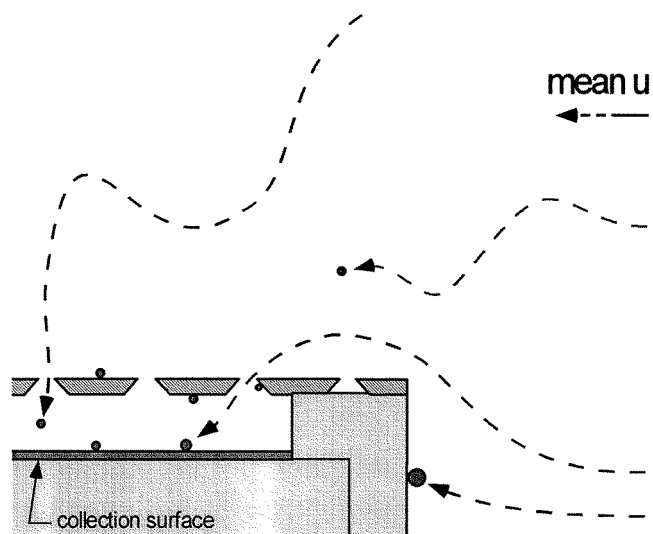


Figure 2. Schematic of deposition into passive sampler with horizontal mean wind velocity.

removed by the hole walls due to inertia, diffusion and interception. Once inside the collection region, some particles will deposit on the underside of the mesh and the collection region walls, enhanced by any air circulations induced inside the collection region. Diffusive deposition inside the collection region may also be influenced by the aerosol concentration inside the collection region.

Expressions analogous to some of these deposition mechanisms have been published in the literature, e.g., enhanced deposition due to surface roughness (Wood 1981), deposition inside a closed vessel (Crump and Seinfeld 1981), and deposition in nucleopore filter holes (Heidam 1981). These expressions apply only loosely to the passive sampler's geometry and flow fields, however, and would require assuming values for the variables which could not be measured directly. Thus using a purely mechanistic equation for the deposition velocity was judged to be inappropriate.

We have adopted an alternative approach, conceptually dividing the overall deposition velocity into two components. The first is the ambient deposition velocity, v_{amb} , which describes the deposition velocity a particle would normally have when depositing onto a flat, smooth surface. This component is expressed as a mechanistic equation. The second component is the "mesh factor," γ_m , an empirical correction which is intended to account for the combined effects of the sampler and mesh, as discussed above. The overall deposition velocity is then expressed as

$$v_{dep} = v_{amb}\gamma_m. \quad [2]$$

The expression for v_{amb} is obtained using a procedure similar to that used by Shimada et al. (1989) and Schneider et al. (1994). For deposition onto a horizontal surface due to turbulent forces

and gravity, one can set up the steady-state equation

$$F_{amb} = v_{amb}C = (D + D_e)\frac{dc}{dy} + v_t c, \quad [3]$$

where F_{amb} is the mass flux onto the surface, $D(= kTC_c/3\pi\mu d_{es})$ is the Brownian diffusion coefficient, k is the Boltzmann constant, T is the ambient temperature, C_c is the Cunningham correction factor, μ is the dynamic viscosity, D_e is the turbulent eddy diffusion coefficient, c is the concentration at height y above the surface, $v_t(= \tau g)$ is the terminal settling velocity, $\tau = (\rho_0 d_a^2 C_c)/(18\mu)$, ρ_0 is the unit particle density, and g is the gravitational acceleration. The equivalent-surface diameter, d_{es} , is the diameter of a sphere with the same surface area as the particle. The aerodynamic diameter, d_a is the diameter of a unit density sphere with the same settling velocity as the particle.

To integrate Equation (3), the terms can be rearranged and converted into dimensionless form:

$$\int_{c_{\sigma+}^+}^1 \frac{dc^+}{v_{amb}^+ - v_t^+ c^+} = \int_{\sigma+}^{\infty} \frac{dy^+}{D^+ + D_e^+}, \quad [4]$$

where $c^+ = (c/C)$, $v_{amb}^+ = (v_{amb}/u_*)$, $v_t^+ = (v_t/u_*)$, $y^+ = (yu_*/\nu)$, $D^+ = (D/\nu)$, $D_e^+ = (D_e/\nu)$, ν is the kinematic viscosity, and u_* is the turbulent friction velocity. Integration is carried out from infinity, where $c^+ = (C/C = 1)$, to a distance from the surface equal to the particle's stop distance, σ . After integrating the left-hand side, one obtains

$$\frac{-1}{v_t^+} [\ln(v_{amb}^+ - v_t^+(1)) - \ln(v_{amb}^+ - v_t^+(c_{\sigma+}^+))] = I^+, \quad [5]$$

where I^+ denotes the integral on the right-hand side of Equation (4). Rearranging terms yields

$$v_{amb}^+ = \frac{v_t^+(1 - c_{\sigma+}^+ e^{-v_t^+ I^+})}{1 - e^{-v_t^+ I^+}}. \quad [6]$$

Assuming steady-state, the fluxes at infinity and at σ from the surface are equal. Then

$$c_{\sigma+}^+ = \frac{v_{amb}^+ \times 1}{v_0^+}, \quad [7]$$

where v_0^+ is the nondimensional velocity of a particle at a distance of σ from the wall. Substituting Equation (7) into Equation (6) and rearranging yields

$$v_{amb}^+ = \frac{-v_t^+}{\left[\left(1 - \frac{v_t^+}{v_0^+}\right)e^{-v_t^+ I^+}\right] - 1}. \quad [8]$$

The expression for I^+ can be adapted from the work of Wood (1981):

$$I^+ = \frac{1}{\frac{3\sqrt{3}}{29\pi} S_c^{-2/3} + 6.2 \times 10^{-4} (\tau^+)^2}, \quad [9]$$

where S_c is the Schmidt number ($= \nu/D$), $\tau^+ = (\tau u_*^2/\nu)$ and the surface is assumed to be smooth.

An empirical expression for v_0^+ was developed by Sehmel (1970):

$$v_0^+ = 1.49(\tau^+)^{-0.49}. \quad [10]$$

Finally, substituting Equation (10) into Equation (8) and converting back to dimensional form yields

$$v_{amb} = \frac{-v_t}{\left[\left(1 - 0.67\tau^{0.49} u_*^{-0.02} \nu^{-0.49} v_t\right)e^{-v_t I}\right] - 1}, \quad [11]$$

where $I = (I^+/u_*)$ and I^+ is given by Equation (9).

To estimate u_* , one can use the correlation

$$u_* = \frac{u}{\ln\left(\frac{z}{z_0}\right)}, \quad [12]$$

where u is the wind speed at height z above the ground and z_0 is the surface roughness. Various authors have compiled values for z_0 corresponding to different surfaces (e.g., Sehmel 1980; McRae et al. 1982), and u can be estimated by consulting data relevant to the given indoor, workplace, or ambient environment. Depending on the sampling application, these data may include previous measurements conducted at the site, literature results for a similar environment, or public-access meteorological data.

When $u_* < 0.4$ m/s, an important simplification to Equation (11) can be made. Figure 3 is a plot of v_{amb} vs. d_a for values of u_* from 0.2 to 0.8 m/s. The figure shows that for $u_* < 0.4$ m/s, the ambient deposition velocity is largely independent of u_* and

$$v_{amb} \cong v_t \quad [13]$$

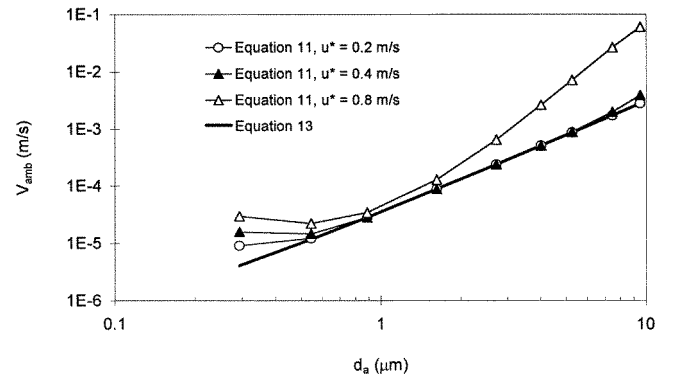


Figure 3. Deposition velocity, v_{dep} , versus aerodynamic particle diameter, d_a , plotted for various friction velocities, u_* .

for $d_a > 0.5 \mu\text{m}$. The simplification can be assumed to hold for all d_a when calculating PM2.5 and PM10, since these mass metrics usually will be dominated by particles with $d_a > 0.5 \mu\text{m}$.

Equation (13) can be used to approximate Equation (11) in many cases. In U.S. outdoor environments, $u = 4 \text{ m/s}$ (at $z = 10 \text{ m}$) is a representative wind speed. Using this wind speed and Equation (12), one finds that $u_* < 0.44 \text{ m/s}$ over all surfaces with $z_0 < 2.6 \text{ cm}$. This z_0 range corresponds to nonurban and nontree-covered areas (McRae et al. 1982). In indoor environments, typical wind speeds are much lower, on the order of $u = 0.1 \text{ m/s}$. Thus Equation (13) should be applicable in some outdoor and most indoor sampling applications.

The expression for γ_m has been determined experimentally in a wind tunnel:

$$\begin{cases} \gamma_m = 1, & d_a < 1.63 \mu\text{m}, \\ \gamma_m = (5.95 \times 10^{-3}) Re_p^{-0.439}, & d_a \geq 1.63 \mu\text{m}, \end{cases} \quad [14]$$

where $Re_p = (d_a v_i / \nu)$. The methods used for this determination are described in detail by Wagner and Leith (2001).

ANALYSIS

After sampling is completed, the passive sampler is transported to the lab in a protective case. In the lab, the case is opened, the mesh cap is removed, and the remaining substrate is then ready for analysis. Analysis of the collected particles can be performed with several different microscopy techniques. Environmental SEM or atomic force microscopy can be utilized to count particles at ambient pressure. With a modified collection substrate, transmission electron microscopy techniques such as cluster analysis, spot-reaction sulfur identification, or EELS spectroscopy could be used (Mamane and de Pena 1978; Saucy et al. 1987; Maynard 1995). An SEM and energy-dispersive x-ray detector were used by Wagner and Leith (2001). SEM is appropriate when the major aerosol constituents are nonvolatile. The energy-dispersive x-ray detector is useful for identifying elements with atomic numbers of 11 and greater. In addition to making an inventory of the elements present in the total collected sample, the chemical compositions of individual particles can be examined in conjunction with their morphology to make inferences about their sources.

To measure the deposition flux as a function of particle size, multiple microscope images are captured by computer at several different magnifications. Fields are selected across the sampler substrate in a random manner, and the particles are semiautomatically counted and sized with the aid of an image analysis software package.

A decision rule is used to count and size particles that are only partially within a given SEM field. Borders of width W , corresponding to the largest particle size expected to be present, are applied to the bottom and right sides of each SEM field. All particles touching these two borders are sized, while all particles touching the other two sides are not. The maximum measurable particle size is then equal to W . At the highest magnifications,

W is not allowed to exceed 1/8 of the field height. In addition, a minimum measurable particle size of $d_p = 7$ pixels is set for all magnifications to prevent inaccurate sizing of small particles.

After counting, both the deposition model and count distribution are discretized into size bins. The number and width of size bins is arbitrary; for comparison of results with those from another sampler, one can create size bins that match those of the other sampler. The mass flux for size bin i is then

$$F_i = \frac{N_i \pi (\bar{d}_{ev})_i^3 \rho_p}{6 A_i t}, \quad [15]$$

where N_i is the number of particles counted in size bin i , ρ_p is the particle density, and t is the sampling time. The total field area used for counting, A_i , varies with particle size because for any given magnification, some size bins will not be within measurement limits. For these size bins, the magnification's field area is not counted. The equivalent-volume diameter, d_{ev} , is the diameter of a sphere with the same volume as the particle. The 3rd moment average, \bar{d}_{ev} , is used to give the average mass of the size bin:

$$\bar{d}_{ev} = \left[\frac{\int_{(d_{ev})_{i,L}}^{(d_{ev})_{i,h}} d_{ev}^3 dd_{ev}}{\int_{(d_{ev})_{i,L}}^{(d_{ev})_{i,h}} dd_{ev}} \right]^{1/3} = \left[\frac{(d_{ev})_{i,h}^4 - (d_{ev})_{i,L}^4}{4((d_{ev})_{i,h} - (d_{ev})_{i,L})} \right]^{1/3}, \quad [16]$$

where $(d_{ev})_{i,L}$ and $(d_{ev})_{i,h}$ are the lower and upper limits of size bin i .

Because many particles are nonspherical, their sizes are measured in terms of their projected area diameters (d_{pa} is the diameter of a sphere with the same projected area as the particle). The d_{pa} values are then converted to d_{es} , d_{ev} , and d_a . These conversions are made using the following expressions (Davies 1979; Noll et al. 1988):

$$d_{es} = d_{pa} \left(\frac{f}{\pi} \right)^{1/2}, \quad [17]$$

$$d_{ev} = \frac{d_{pa}}{S_v}, \quad [18]$$

$$d_a = d_{ev} \left(\frac{\rho_p C_{c,dev}}{\rho_o C_{c,da}} \frac{1}{S_d} \right)^{1/2}. \quad [19]$$

where f is the surface shape factor, S_v is the volume shape factor, and S_d is the dynamic shape factor. Equations (18) and (19) can be combined to give

$$\frac{d_a}{d_{pa}} = \left(\frac{C_{c,dev}}{C_{c,da}} \right)^{1/2} \left(\frac{\rho_p}{\rho_o} \frac{1}{S_d} \right)^{1/2} \frac{1}{S_v}. \quad [20]$$

Note that for particle sizes $> 1 \mu\text{m}$, $C_c \cong 1$ and (d_a/d_{pa}) becomes independent of particle size.

Published data can be used to estimate these parameters (Table 1). Except where indicated, all tabulated values are either measured quantities or are derived from measured quantities.

Table 1

Shape factors and densities for various particle types [D = Davies (1979); C = CRC (1997); S = Stein et al. (1969); N = Noll et al. (1988); L = Lin et al. (1994); H = Hinds (1982)]

Particle type	Ref.	ρ_p (g/cm ³)	S_v	S_d	f	d_a/d_{pa}^a
Common dusts						
Quartz	D	2.65	1.2–1.4	1.36	2.4	0.97–1.16
Sand	D	2.5	1.3	1.57	2.95	1.0
China clay	D	2.2	—	—	—	0.92
Talc	D	2.6	1.5	2.04	2.18	0.73–0.77
Anthracite coal	D	1.5	1.5	1.37	2.2	0.70
Bituminous coal	D	1.4	1.3	1.05–1.11	3.02	0.87–0.90
Glass	D	2.6	—	—	—	1.08–1.34
Cotton	D	1.5	—	—	—	0.72–0.78
Limestone (CaCO ₃)	C/D	2.7	1.5	—	—	—
Gypsum (CaSO ₄ ·2H ₂ O)	C/D	2.3	1.6	—	—	—
Heterogeneous aerosols						
1969 Pittsburgh aerosol	S	2.2	—	—	—	0.68
1986 Chicago aerosol	N	2.0 ^b	1.89	1.41 ^b	—	0.63 ^c
1992 Chicago aerosol	L	1.77 (fine) ^b 2.64 (coarse) ^b	1.61	1.41 ^b	—	0.74 ^c
General shapes						
Sphere	H	[1.0]	1.00	1.00	3.14	1.00
Cube	H	[1.0]	1.11	1.02	—	0.89
Compact flake	D	—	1.34	—	2.38	—

^aFor $d_p < 1 \mu\text{m}$, multiply value by (C_{cdev}/C_{cda}) .

^bEstimated, not measured.

^cCalculated using estimated parameter.

To use Table 1, one must have some knowledge of the aerosol sample's identity. This information can be obtained from the microscopy and x-ray fluorescence. In some cases, the aerosol's composition may be homogenous or well specified, e.g., when sampling in certain industrial environments. In many cases, however, average parameter values must be assumed for a fairly heterogeneous aerosol. For example, a value of $\rho_p = 2.0 \text{ g/cm}^3$ has been selected as an average value when sampling urban atmospheric aerosols (Noll et al. 1988). Lin et al. (1994) estimated different densities for fine and coarse particles based on their respective primary components, $(\text{NH}_4)_2\text{SO}_4$ and SiO_2 .

Once average aerosol types have been identified, one can consult Table 1 to obtain f , S_v , and S_d . (If Equation (13) is used, d_{es} does not enter into the calculations and f does not need to be estimated.) For particle types with no listed S_v or S_d values, one can calculate d_a directly using the tabulated d_a/d_{pa} values. In contrast with Equation (20), however, these values are not size dependent and are only valid for particle sizes $> 1 \mu\text{m}$. For particles smaller than $1 \mu\text{m}$, one should multiply the tabulated value by (C_{cdev}/C_{cda}) . Regardless, an estimate of S_v is still required to obtain d_{ev} for use in Equation (15).

To estimate shape factors whose values are not listed in Table 1, one should determine the average shape of the collected particles, i.e., flaky, angular, or rod-like. Then one can estimate S_d or S_v using tabulated values for various particle shapes. Only

the most basic shapes are given in Table 1; many more are given by Davies (1979) and Hinds (1982). In addition, procedures exist for calculating S_d for a given geometric shape (Leith 1987) and for agglomerates (Tohno and Takahashi 1990).

Using the mass flux together with Equations (1), (2), (9), and (11) (or Equations (1), (2), and (13) for $u_* < 0.4 \text{ m/s}$), one can then calculate C for each size bin. The midpoint of each size bin is used to calculate d_{es} in Equation (9). To calculate τ for each size bin \bar{d}_a is used, where

$$\bar{d}_a = \left[\frac{\int_{(d_a)_{i,L}}^{(d_a)_{i,h}} d_a^2 dd_a}{\int_{(d_a)_{i,L}}^{(d_a)_{i,h}} dd_a} \right]^{\frac{1}{2}} = \left[\frac{(d_a)_{i,h}^3 - (d_a)_{i,L}^3}{3((d_a)_{i,h} - (d_a)_{i,L})} \right]^{\frac{1}{2}} \quad [21]$$

and $(d_a)_{i,L}$ and $(d_a)_{i,h}$ are the lower and upper limits of size bin i .

CONCLUSION

A method has been developed to estimate average concentrations and size distributions with a passive aerosol sampler. To use the passive sampler, one exposes it to an environment for a period of hours to weeks. The sampler is then covered and brought to the lab. Microscopy and image analysis are used in conjunction with particle density and shape factors to obtain the mass flux as a function of aerodynamic diameter. The flux and a

deposition velocity model are then used to calculate the average concentration and size distribution to which the sampler was exposed.

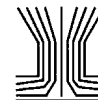
The deposition velocity model consists of a theoretical component and an empirical component. The theoretical component incorporates gravitational, inertial, and diffusive mechanisms, but can be approximated by the simple terminal settling velocity in many cases. Wagner and Leith (2001) describe the determination of the empirical component and give the results of laboratory tests of the passive sampler's precision. Field testing is now underway in an occupational environment.

ACKNOWLEDGMENTS

The authors wish to thank the National Institute for Occupational Safety and Health (1 R03 OHO3774-01), the U.S. Environmental Protection Agency (U-915321-01-0), the National Institute of Environmental Health Sciences (5 T32 ES07018-21), the U.S. Department of Education (P200A40274-96), and the UNC Board of Governors for supporting this work.

REFERENCES

- Brown, R. C., Hemingway, M. A., Wake, D., and Thompson, J. (1995). Field Trials of an Electret-Based Passive Dust Sampler in Metal-Processing Industries, *Ann. Occup. Hyg.* 39:603–622.
- Brown, R. C., Hemingway, M. A., Wake, D., and Thorpe, A. (1996). Electret-Based Passive Dust Sampler: Sampling of Organic Dusts, *Analyst* 121:1241–1246.
- Cooper, D. W., Peters, M. H., and Miller, R. J. (1989). Predicted Deposition of Submicrometer Particles Due to Diffusion and Electrostatics in Viscous Axisymmetric Stagnation-Point Flow, *Aerosol Sci. Technol.* 11:133–143.
- CRC. (1997). *Handbook of Chemistry and Physics*, 77th Ed., CRC Press, Boca Raton, FL, pp. 15–29.
- Crump, J. G., and Seinfeld, J. H. (1981). Turbulent Deposition and Gravitational Sedimentation of an Aerosol in a Vessel of Arbitrary Shape, *J. Aerosol Sci.* 12:405–415.
- Davies, C. N. (1979). Particle-Fluid Interaction, *J. Aerosol Sci.* 10:477–513.
- Dockery, D. W., Pope, C. A., Xu, X., Spengler, J. D., Ware, J. H., Fay, M. E., Ferris, B. G., and Speizer, F. E. (1993). An Association Between Air Pollution and Mortality in Six U.S. Cities, *N. Engl. J. Med.* 329:1753–1759.
- Heidam, N. Z. (1981). Review: Aerosol Fractionation by Sequential Filtration by Nuclepore Filters, *Atmospheric Environment* 15:891–904.
- Hinds, W. C. (1982). *Aerosol Technology*, John Wiley and Sons, New York, pp. 48, 365.
- Lehtimäki, M., and Willeke, K. (1993). Measurement Methods. In *Aerosol Measurement: Principles, Techniques, and Applications*, edited by K. Willeke and P. A. Baron. Van Nostrand Reinhold, New York, pp. 115.
- Leith, D. (1987). Drag on Nonspherical objects, *Aerosol Sci. Technol.* 6:153–161.
- Lin, J., Noll, K. E., and Holsen, T. M. (1994). Dry Deposition Velocities as a Function of Particle Size in the Ambient Atmosphere, *Aerosol Sci. Technol.* 20:239–252.
- Liu, B. Y. H., and Ahn, K. (1987). Particle Deposition on Semiconductor Wafers, *Aerosol Sci. Technol.* 6:215–224.
- Liu, L., Koutrakis, P., Leech, J., and Broder, I. (1995). Assessment of Ozone Exposures in the Greater Metropolitan Toronto Area, *J. Air & Waste Manage. Assoc.* 45:223–224.
- Mamane, Y., and DePena, R. G. (1978). A Quantitative Method for the Detection of Individual Submicrometer Size Sulfate Particles, *Atmospheric Environment* 12:69–82.
- Maynard, A. D. (1995). The Application of Electron Energy-Loss Spectroscopy to the Analysis of Ultrafine Aerosol Particles, *J. Aerosol Sci.* 26:757–777.
- McMurry, P. H., and Rader, D. J. (1985). Aerosol Wall Losses in Electrically Charged Chambers, *Aerosol Sci. Technol.* 4:249–268.
- McRae, G. J., Goodwin, W. R., and Seinfeld, J. H. (1982). Development of a Second-Generation Mathematical Model for Urban Air Pollution-I, *Atmospheric Environment* 16:679–696.
- Nazaroff, W. W., and Cass, G. R. (1987). Particle Deposition from a Natural Convection Flow onto a Vertical Isothermal Flat Plate, *J. Aerosol Sci.* 18:445–455.
- Noll, K. E., Fang, K. Y. P., and Watkins, L. A. (1988). Characterization of the Deposition of Particles from the Atmosphere to a Flat Plate, *Atmospheric Environment* 22:1461–1468.
- Pope, C. A., Thun, M. J., Namboori, M. M., Dockery, D. W., Evans, J. S., Speizer, F. E., and Heath, C. W. (1995). Particulate Air Pollution as a Predictor of Mortality in a Prospective Study of U.S. Adults, *Am. J. Respir. Crit. Care Med.* 151:669–674.
- Rappaport, S. M. (1994). Interpreting Levels of Exposures to Chemical Agents. In *Patty's Industrial Hygiene and Toxicology, Third Edition, Volume 3, Part A*, edited by R. L. Harris, L. J. Cralley, and L. V. Cralley. John Wiley and Sons, New York, pp. 349–403.
- Saucy, D. A., Anderson, J. R., and Buseck, P. R. (1987). Cluster Analysis Applied to Atmospheric Aerosol Samples from the Norwegian Arctic, *Atmospheric Environment* 21:1649–1657.
- Schneider, T., Bohgard, M., and Gudmundsson, A. (1994). A semiempirical Model for Particle Deposition onto Facial Skin and Eyes. Role of Air Currents and Electric Fields, *J. Aerosol Sci.* 25:583–593.
- Sehmel, G. A. (1970). Particle Deposition from Turbulent Air Flow, *J. Geophys. Res.* 75:1766–1781.
- Sehmel, G. A. (1980). Particle and Gas Dry deposition: A Review, *Atmospheric Environment* 14:983–1011.
- Sehmel, G. A., and Hodgson, W. J. (1978). *A Model for Predicting Dry Deposition of Particles and Gases to Environmental Surfaces*, PNL-SA-6721, Battelle, Pacific Northwest Laboratory, Richland, WA.
- Shimada, M., Okuyama, K., and Kousaka, Y. (1989). Influence of Particle Inertia on Aerosol Deposition in a Stirred Turbulent Flow Field, *J. Aerosol Sci.* 20:419–429.
- Slinn, S. A., and Slinn, W. G. N. (1980). Predictions for Particle Deposition on Natural Waters, *Atmospheric Environment* 14:1013–1016.
- Stein, F., Esmen, N. A., and Corn, M. (1969). The Shape of Atmospheric Particles in Pittsburgh Air, *Atmospheric Environment* 3:443–453.
- Suh, H. H., Spengler, J. D., and Koutrakis, P. (1992). Personal Exposures to Acid Aerosols and Ammonia, *Environ. Sci. Technol.* 26:2507–2517.
- Thurston, G. D., Ito, K., Hayes, C. G., Bates, D. V., and Lippman, M. (1994). Respiratory Hospital Admissions and Summertime Haze Air Pollution in Toronto, Ontario: Consideration of the Role of Acid Aerosols, *Environ. Res.* 65:271–290.
- Tohno, S., and Takahashi, K. (1990). Morphological and Dynamic Characterization of Pb Fume Particles Undergoing Brownian Coagulation, *J. Aerosol Sci.* 21:719–732.
- Vinzents, P. S. (1996). A Personal Passive Dust Monitor, *Ann. Occup. Hyg.* 40:261–280.
- Wagner, J., and Leith, D. (2001). Passive Aerosol Sampler. Part II: Wind Tunnel Experiments, *Aerosol Sci. Technol.* (see subsequent article in this issue).
- Wiener, R. W., and Rodes, C. E. (1993). Indoor Aerosols and Aerosol Exposure. In *Aerosol Measurement: Principles, Techniques, and Applications*, edited by K. Willeke and P. A. Baron. Van Nostrand Reinhold, New York, pp. 659–689.
- Wood, N. B. (1981). A Simple Method for the Calculation of Turbulent Deposition to Smooth and Rough Surfaces, *J. Aerosol Sci.* 12:275–290.



Passive Aerosol Sampler. Part II: Wind Tunnel Experiments

Jeff Wagner and David Leith

University of North Carolina, Department of Environmental Sciences and Engineering,
Chapel Hill, North Carolina

Wind tunnel experiments have been performed on a passive aerosol sampler. The sampler estimates average concentrations and size distributions using a deposition velocity model and the measured particle flux to the sampler. The small-scale wind tunnel incorporated a high-output aerosol generator that produced nonvolatile, polydisperse particles. An eight-stage impactor was connected to the tunnel with an isoaxial, isokinetic probe and was equipped with polycarbonate-membrane substrates saturated with oleic acid to minimize particle bounce. Before performing experiments, the tunnel's test section was characterized. Aerosol concentrations were determined to have a CV < 6%. The friction velocity, an index of turbulence, was found to range from 0.09 to 0.25 m/s for wind speeds of 1.5 to 5 m/s. The empirical portion of the deposition velocity model, γ_m , was determined as a function of particle size by minimizing the sum-of-squares difference between impactor and passive sampler across all size bins and all experiments. The relatively simple correlation is a function of the particle Reynolds number only. Precision was assessed by running three passive samplers simultaneously in each experiment. The tests yielded $CV_{PM2.5} = 18.1\%$ and $CV_{PM10} = 32.2\%$. ANOVA tests were conducted on accuracy and precision to see whether they depended on wind speed, relative humidity, or aerosol concentration, and accuracy was tested with respect to particle size. No significant trends were observed. Sensitivity analysis showed that the volume shape factor is the most important of the mass and shape conversion factors. If SEM is used, the passive sampler will exhibit some error when sampling volatile aerosols. Because concentrations fluctuate over time, long-term exposures measured by the passive sampler should be more accurate than conventional averages based on short-term samples.

INTRODUCTION

The overall objective of this research is to develop a miniature passive aerosol sampler to estimate average size distributions and concentrations. The passive sampler monitors ambient, indoor, or occupational aerosols over periods of hours to weeks and

is about the size of a dime. During sampling, particles passively deposit on the collection surface. Scanning electron microscopy (SEM) or other microscopy techniques are then used to analyze the collected particles (Wagner and Leith 2001).

Mass size distributions are calculated by dividing the measured mass flux, F , by the deposition velocity, v_{dep} :

$$C = \frac{F}{v_{dep}} = \frac{F}{v_{amb}\gamma_m} \quad [1]$$

where C is the average mass concentration over the sampling period, v_{amb} is the ambient deposition velocity, and γ_m is the mesh factor. All are calculated as a function of aerodynamic diameter, d_a . Standard measures of airborne particulate levels such as PM_{2.5} and PM₁₀ (mass concentration of particles with aerodynamic diameters <2.5 μm and 10 μm , respectively) can be calculated by integrating C over the appropriate particle sizes.

A special wind tunnel was designed and built to test the passive sampler. The wind tunnel tests were used to determine γ_m under different wind conditions and to determine the precision of the passive sampler.

This paper begins by describing the rationale for these tests and the design of the wind tunnel. Next, the characterization of the wind tunnel's concentration and flow fields is described. Methods, results, and discussion of the passive sampler tests follow. The paper concludes with sensitivity and uncertainty analyses.

WIND TUNNEL DESIGN

Test Objectives and Rationale

The objectives of the wind tunnel tests were to determine γ_m under different wind conditions and to determine the precision of the passive sampler. The empirical expression for γ_m was determined by fitting the size distribution results of the passive sampler to those of an active, mass-based sampler. Because "accuracy" has been defined with respect to the reference sampler, an effort was made to reduce the reference sampler's uncertainties as much as possible. Precision was assessed by testing

Received 13 April 1999; accepted 10 December 1999.

Address correspondence to Jeff Wagner, Department of Environmental Sciences and Engineering, CB#7400, Rosenau Hall, Chapel Hill, NC 27599. E-mail: jr.wagner@lbl.gov

three passive samplers simultaneously. A secondary objective was to determine if γ_m was dependent on the relative humidity or aerosol concentration.

Although many approaches are possible when testing a sampler, a decision was made to test under defined, stable conditions. The effect of more realistic, fluctuating conditions will be assessed separately with field tests. Experiments were designed for a range of constant wind speeds and an aerosol with known properties. The two major variables of the experiments were then wind speed and particle size.

Unique Features of the Wind Tunnel

Because testing of the passive sampler required some unique conditions, a special wind tunnel was designed and built.

Several criteria had to be met for the aerosol generator and test aerosol. For one, the passive sampler is designed to sample over a period of weeks. To scale down experiment times so that they were on the order of hours, it was necessary to scale up the aerosol concentrations accordingly. Thus an aerosol generator capable of producing sustained high concentrations was needed, as well as a large quantity of particulate matter. Because analyses were conducted under vacuum with an SEM, a nonvolatile aerosol was needed. Finally, the test aerosol had to be polydisperse, with a portion in the submicron range.

To satisfy these criteria, a HEART high-output nebulizer (Westmed, Inc., Tuscon, AZ) was used to disperse continuously a slurry of distilled water and a manufactured SiO₂ dust (CERAC, Milwaukee, WI). A Kr-85 neutralizer (Model 3054, TSI Inc., St. Paul, MN) was used to neutralize the aerosol immediately downstream of the nebulizer. Because the output of the nebulizer was 12 LPM, or less than one tenth of the neutralizer's maximum recommended flow rate, the aerosol was assumed to be fully neutralized. The nebulized SiO₂ dust had a size range of approximately (0.6–9) μm , and an average of 13 g SiO₂/200 ml H₂O was nebulized per experiment. The original size distribution of the SiO₂ was slightly undesirable in that it had too many coarse particles. The distribution was improved by injecting the nebulized aerosol near the bottom of one end of the tunnel, removing many of the coarse particles as the aerosol traveled toward the test section at the other end. Using this apparatus, concentrations of up to 7.4 mg/m³ were maintained in the tunnel's test section for 2–7 h, with an average mass median aerodynamic diameter of 2.5 μm and geometric standard deviation of 1.8.

To achieve high concentrations at wind speeds of up to 5 m/s, the wind tunnel was built with a small cross-section (50 × 100) mm. Because the passive samplers are also quite small, placing three passive samplers side by side in the tunnel was feasible. Using a smaller cross section also made it easier to maintain a uniform concentration profile than would be possible with a conventional, larger wind tunnel (Ramachandran et al. 1998).

The reference sampler was an eight-stage Andersen cascade impactor (Andersen Instruments Inc., Smyrna, GA) with size cuts between (0.43–9) μm and a 10 μm preseparator. To min-

imize particle bounce, a 77 mm polycarbonate membrane substrate with 5.0 μm pore size was placed on each impactor stage and saturated with 20 μL oleic acid. The substrates were trimmed down from 90 mm Isopore filters (Millipore, Bedford, MA). This approach was based on the work of Turner and Hering (1987). The impactor was equipped with a probe mounted isoaxially with the tunnel flow. Interchangeable probe inlets were used to sample isokinetically at each wind speed.

Overview of Wind Tunnel

A schematic of the wind tunnel is shown in Figure 1. The straight section of the tunnel was constructed of clear acrylic, had a rectangular cross section, and was 2.4 m long. Air was pulled through the straight section by two high-volume samplers (hivols) in parallel. Wind speeds in the tunnel were adjusted by variable transformers connected to the hivols and were monitored with a hot-film anemometer (Velocichck Model 8830, TSI Inc., St. Paul, MN).

Aerosol was injected at the bottom of the entrance to the tunnel. The aerosol then encountered turbulence screens at 51 and 56 cm downstream. The screens had wire spacings of 1.2 cm and 0.2 cm, respectively. The first screen was blocked across the bottom half to create a flow "hurdle." This feature enhanced particle mixing into the upper half of the tunnel cross section. After travelling the length of the straight section, the aerosol encountered the test section. There, three passive samplers were mounted side by side in a holder in the mid-plane of the tunnel. The samplers' collection surfaces were parallel to the flow, and the samplers were electrically grounded. The inlet to the impactor probe was mounted 6.5 cm behind the passive samplers, also in the mid-plane of the tunnel. Finally, the aerosol traveled around a 45° elbow through a filter holder and hivol manifold. The unit consisting of the hivol manifold, filter holder, and impactor apparatus was mounted on a wheeled cart that could be detached from the rest of the wind tunnel.

Aerosol concentrations in the wind tunnel were monitored qualitatively with one of two real-time optical aerosol monitors, either a DataRAM (MIE Inc., Billerica, MA) or DustTRAK (TSI Inc., St. Paul, MN). Relative humidity in the tunnel was monitored with a dew point hygrometer (Model 11-661, Fisher Scientific, Atlanta, GA).

WIND TUNNEL CHARACTERIZATION

Spatial Uniformity of Aerosol

A valid comparison between two samplers requires that both be exposed to comparable aerosols. Because the passive samplers were located 6.5 cm away from the impactor's probe inlet, establishing spatial uniformity in the test section was important. Spatial uniformity of the aerosol was characterized with an Aerosizer LD (API, Hadley, MA), a time-of-flight particle sizer. Aerosol measurements were taken at 18 points across two equal area 3 × 3 traverse planes (Figure 2). The first plane was located 3.2 cm upstream of the samplers, while the second

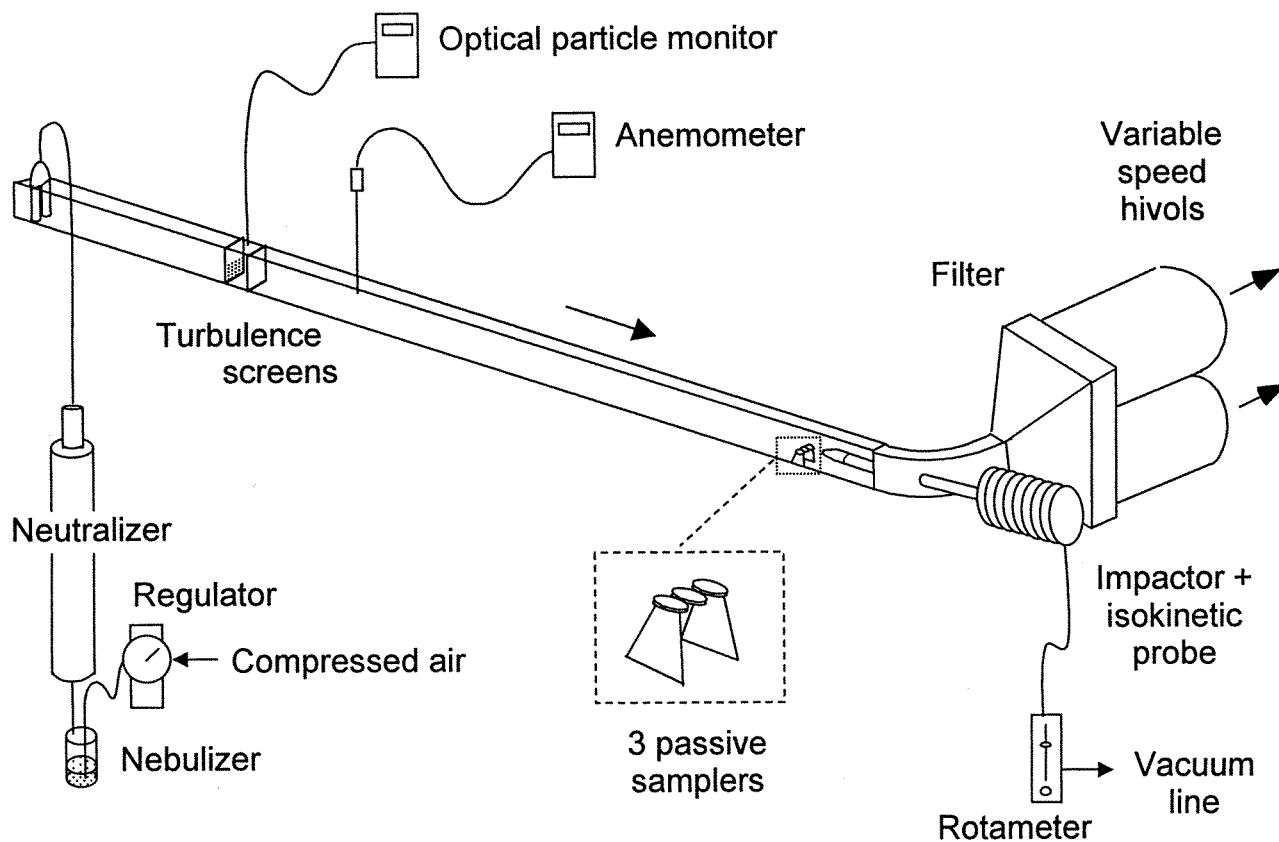


Figure 1. Wind tunnel for testing passive samplers.

plane was located between the passive samplers and the impactor probe, 2 cm downstream of the passive samplers. Three sets of replicates were performed at each location, for a total of 54 measurements. The aerosol used for these tests was a lactose aerosol with a measured aerodynamic size range of approximately $0.2\text{--}4\ \mu\text{m}$ and a mass median aerodynamic diameter of $1.0\ \mu\text{m}$. Sampling was performed by inserting a small, grounded copper probe (7.5 cm long, ID = 5 mm) into sampling ports on the side of the tunnel. The probe had a 90° elbow so that the inlet was parallel to the flow direction. The passive samplers were

mounted on the tunnel floor during these tests. Measurements were taken at the lowest tunnel wind speed used in the passive sampler experiments, $u = 1.5\ \text{m/s}$, to achieve a “worst case” mixing of the aerosol.

For total mass concentration, small but significant differences were found between positions and as a function of height above the tunnel floor. The coefficient of variation (CV) between positions was fairly low: $\text{CV} = 5.6\%$. In addition, only 28% of the 153 pairwise comparisons between positions showed significant differences. Average concentrations across the two traverse planes were not significantly different.

The diameter of average mass was also calculated for each measured size distribution. No significant differences were found between positions or with height. The CV between positions and all CVs within position were very low, $<1\%$.

A limitation of this characterization is that most measured particles had an aerodynamic diameter of $d_a < 4\ \mu\text{m}$. Larger particles could exhibit more spatial variability than described above, although approximately 70% of the aerosol mass in the passive sampler experiments described later was also $<4\ \mu\text{m}$. To further reduce the effects of any variability, the passive sampler mount was modified for subsequent experiments so that the samplers were at the same height as the impactor probe. Thus the aerosols measured by the passive samplers and the impactor were judged to be reasonably comparable and suitable for further work.

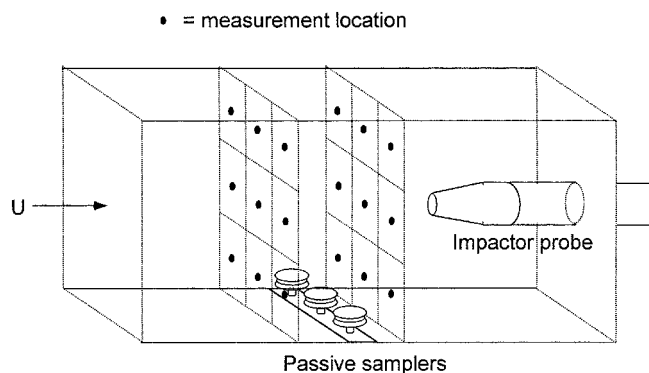


Figure 2. Traverses used for concentration uniformity measurements.

Turbulence Characterization

Because the tunnel's reference sampler was active rather than passive, it was not appropriate to establish that both sampler types experienced comparable flow fields. Instead, each sampler type had different flow considerations. The impactor required isokinetic and isoaxial sampling conditions. At the start of each experiment, the velocity adjacent to the probe inlet was measured with a hot-film anemometer (Velocichck Model 8830, TSI, Inc., St. Paul, MN). The probe alignment and tunnel wind speed were then adjusted so that the tunnel velocity was equal in magnitude and direction to the probe inlet velocity.

For the passive sampler, it was necessary to characterize the friction velocity, u_* , in the test section. This parameter is an index of the turbulence and is required for development of the deposition velocity model. At each of the four experimental wind speeds, vertical velocity profiles were measured upstream of the passive samplers in the center of the tunnel cross section. Velocity profiles were measured with a platinum hot-film anemometer (Model 1240-20, TSI Inc., St. Paul, MN) and controller/signal processor (IFA-100 Intelligent Flow Analyzer, TSI Inc., St. Paul, MN). The anemometer was calibrated in a 0.20 m diameter flanged duct with an orifice meter.

Each velocity profile consisted of 6 pairs of replicate measurements of the mean streamwise component of the velocity. Because calculations showed that the flow was in the "hydraulically smooth" regime, an equation for the velocity profile in a smooth pipe was then adapted from Schlichting (1979):

$$u(y_{e\alpha}) = u_* \left[2.5 \ln \left(\frac{y_{e\alpha} u_*}{\nu} \right) + 5.5 \right], \quad [2]$$

where $u(y_{e\alpha})$ is the wind speed at a distance $y_{e\alpha}$ from the tunnel walls, ν is the kinematic viscosity, $y_{e\alpha} = (yD_h/H)$, y is the actual vertical distance, H is the vertical height of the tunnel, $D_h = (4A/P_w)$ is the hydraulic diameter, A is the cross-sectional area of the tunnel, and P_w is the wetted perimeter of the tunnel. The concept of effective distance was used to account for the noncircular tunnel cross section.

By adjusting the value of u_* , Equation (2) could then be fitted to each vertical profile using the method of least squares. An example data fit is shown in Figure 3. This procedure was used to determine u_* empirically as a function of tunnel wind speed (Table 1). Although these u_* values are strictly valid for the center passive sampler only, they were assumed to represent adequately the turbulence near the left and right samplers as well. This assumption was supported by later experiments, which revealed no consistent variation in deposition across the tunnel cross section (see Results).

A regression analysis of the logarithms of u_* and the mean tunnel wind speed, U , yielded

$$u_* = (6.2 \times 10^{-2}) U^{0.88}. \quad [3]$$

For these experiments, $\nu = 1.5 \times 10^{-5} \text{ m}^2/\text{s}$ and $D_h = 0.07 \text{ m}$. Using these values and an equation developed by Blasius for

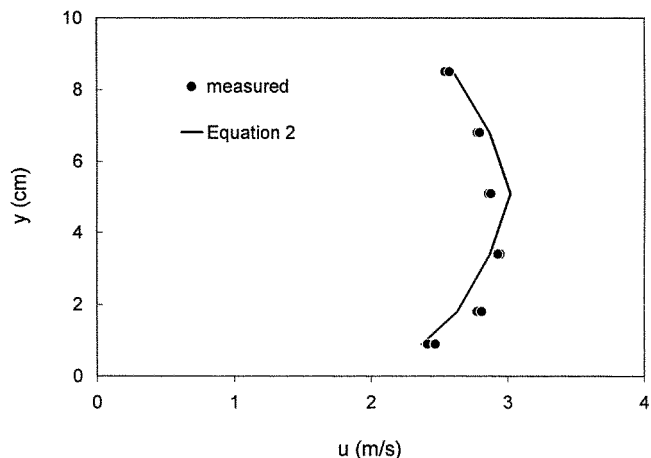


Figure 3. Fit of Equation (2) to a measured velocity profile. For this profile, $u_{avg} = 2.7 \text{ m/s}$ and $u_* = 0.15 \text{ m/s}$.

pipe flow (cited in White (1994)), one obtains

$$u_* = U \left(\frac{0.316 Re_d^{-1/4}}{8} \right)^{1/2} = 0.2U \left(\frac{\nu}{D_h U} \right)^{1/8} = (6.9 \times 10^{-2}) U^{0.875}, \quad [4]$$

where Re_d is the duct Reynolds number. By comparing Equations (3) and (4), one can see that the experimental result found in this study matches that predicted by theory extremely well.

METHODS

Experiment

To prepare the passive samplers for each experiment, four mesh caps, one plastic case, and a section of aluminum tape were cleaned with soap, water, and methanol. The meshes were further cleaned with a fine-haired brush and blasts of compressed air to clear the mesh holes of any debris. Spray mount adhesive was applied to the surfaces of four SEM stubs, and one 7 mm aluminum disc was placed in the center of each stub. After cleaning the discs with methanol, a mesh cap was placed onto each substrate and the samplers were closed inside their plastic case until the experiment began. The fourth passive sampler was used as a sampling blank.

Table 1

Results of wind tunnel turbulence measurements			
Nominal tunnel wind speed (m/s)	Velocity at probe inlet (m/s)	Mean wind speed, U (m/s)	Friction velocity, u_* (m/s)
1.5	1.6	1.5	0.09
3	2.9	2.7	0.15
4	3.9	3.7	0.20
5	5.0	4.9	0.25

Impactor concentrations were obtained gravimetrically with an analytical balance (Mettler Toledo Model AE200, Toledo, OH). Preweighing was conducted at least 1 h after applying oleic acid to the impactor substrates.

Duplicate experiments were run at $u = 1.5, 3, 4,$ and 5 m/s. Concentrations and relative humidities varied randomly between experiments. Relative humidity (RH) and temperature were recorded at the start and end of each experiment with the nebulizer running.

At the end of each experiment, the three passive samplers were returned to their plastic case to stop sampling.

Passive Sampler Analysis

The general analysis procedure is described elsewhere (Wagner and Leith 2001); additional methods and parameters used in the wind tunnel experiments are presented here. Before obtaining images with a Cambridge S-200 SEM (Leo Inc., Fomwood, NY), each passive sampler substrate was sputter-coated with a 60/40% gold/palladium alloy to enhance conductivity and resolution. Counts per area as a function of particle size were obtained for particles with $d_p > 0.1 \mu\text{m}$ using an image acquisition system (Spectral Engine 4.0, 4 Pi Analysis Inc., Durham, NC) and image analysis software (SigmaScan-Pro, Jandel Scientific, San Rafael, CA). An energy-dispersive X-ray detector (KEVX 7000, Fisons, San Carlos, CA) was occasionally used to distinguish submicron SiO_2 particles from the contaminant particles present on the aluminum substrates. Typically, 20-40 SEM fields were acquired across 6 or 7 different magnifications for each sampler. A $10 \mu\text{m}$ border decision rule was used to handle particles that were only partially within a given SEM field.

The continuous count data were discretized into nine size bins to match those of the impactor. To convert the count data to mass fluxes, values of $\rho_p = 2.65 \text{ g/cm}^3$, $S_d = 1.36$, and $S_v = 1.25$ were used for the particle density, dynamic shape factor, and volume shape factor, respectively. These values were taken from published data presented by Davies (1979) for SiO_2 . Some degree of particle agglomeration was found in the SEM images, with the agglomerates tending to be more spherical than

the nonagglomerates. Thus the value for S_v was chosen to be at the upper end of the range of values presented by Davies, i.e., tending towards the more spherical end of the range.

Because $u_* < 0.4$ m/s for all wind tunnel experiments, Equation (1) was calculated using $v_{amb} = v_t = \tau g$, where $\tau = (\rho_0 d_a^2 C_c)/(18 \mu)$, ρ_0 is unit particle density, C_c is the Cunningham correction factor, μ is the dynamic viscosity, and g is the gravitational acceleration (Wagner and Leith 2001).

RESULTS

Experimental conditions for the eight wind tunnel experiments are listed in Table 2. Experiments typically lasted 2-8 h. RHs and temperatures ranged from 15 to 50% and 21 to 27 °C, respectively. Aerosol size distributions measured by the impactor were lognormal. Cumulative log-probability plots showed linear relationships, with regression coefficients of $R^2 \geq 0.99$ for each experiment.

The average number of counts per passive sampler was calculated by dividing the total counts obtained in each experiment by three (Table 2). A typical surface density collected by the passive samplers is shown in Figure 4. Relatively low counts were recorded with the passive samplers because of a limitation imposed by the impactor. Total mass loadings on the impactor substrates of >40 mg led to undesirable amounts of particle bounce, so experiment durations and concentrations had to be kept below certain levels. Evidence of substantial bounce under higher loading conditions included particle deposits in the impactor jets and departures from lognormality in the impactor size distributions. Apparently, collected masses of this magnitude overcame the oleic acid/filter method designed to prevent bounce from occurring. All eight experiments used for analysis had total collected impactor masses of <25 mg.

The mesh factor, γ_m , was determined by comparing impactor concentrations to the averages of the three passive sampler concentrations determined for each experiment. An optimal expression for γ_m was developed by minimizing the sum-of-squares difference between impactor and passive sampler at each size bin, across all experiments. The optimization parameter, OP, was

Table 2
Experimental conditions for passive sampler testing

Test ID	Wind speed (m/s)	Duration (min)	Avg. RH (%)	Avg. temp. (C)	PM10 (mg/m^3)*	MMAD (μm)/GSD*	Avg. count per passive sampler
1	1.5	462	43.2	23.5	1.8	3.1/2.0	60.0
2	1.5	102	14.6	21.5	7.4	2.9/1.9	74.3
3	3	247	16.4	21.1	2.9	2.6/1.7	73.0
4	3	240	22.5	25.6	1.5	2.0/1.8	78.3
5	4	280	50.1	27.0	2.7	2.1/1.5	82.3
6	4	237	15.7	23.0	3.1	2.3/1.8	70.3
7	5	262	20.6	23.3	2.2	2.3/1.8	95.3
8	5	360	30.4	21.8	2.0	2.6/1.9	81.0

*As measured by the impactor.

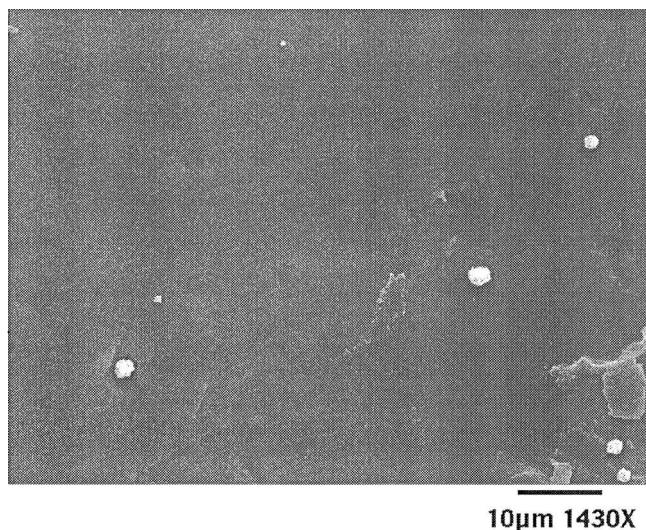


Figure 4. SEM image from passive sample analysis.

defined as follows:

$$OP = \sum_{j=1}^8 \left[\sum_{i=1}^9 \left(\frac{(dC/d \log d_a)_{\text{passive}} - (dC/d \log d_a)_{\text{impactor}}}{(dC/d \log d_a)_{\text{impactor}}} \right)^2 \right]_i \quad [5]$$

where $(dC/d \log d_a)$ is the concentration of size bin i (normalized by the width of the bin) and j is the experiment number. The OP was minimized by formulating γ_m with appropriate dimensionless groups, then determining the constants using the “Solver” tool in Microsoft Excel (Seattle, WA). Data points for which either a) the impactor recorded zero mass or b) the passive sampler average was less than one count per sampler were not included in the optimization. Otherwise, this procedure weighted each size bin equally, independent of the test aerosol’s size distribution.

Several formulations for γ_m were explored, with an emphasis on obtaining the simplest model possible that still provided a good optimization. The following expression was obtained:

$$\begin{cases} \gamma_m = 1, & d_a < 1.63 \mu\text{m}, \\ \gamma_m = (5.95 \times 10^{-3}) Re_p^{-0.439}, & d_a \geq 1.63 \mu\text{m}, \end{cases} \quad [6]$$

where $Re_p = (d_a v_t / \nu)$. This relatively simple expression contains one dimensionless group and three parameters, including the diameter at which γ_m starts to steadily decrease with d_a . Note that this expression is not dependent on u_* and therefore does not require estimating u_* when sampling. Only small variations in deposition were observed as a function of wind speed for the experimental conditions ($u_* < 0.3$ m/s).

Other candidates for γ_m possessed additional parameters and dimensionless groups, including u_* terms. These models gen-

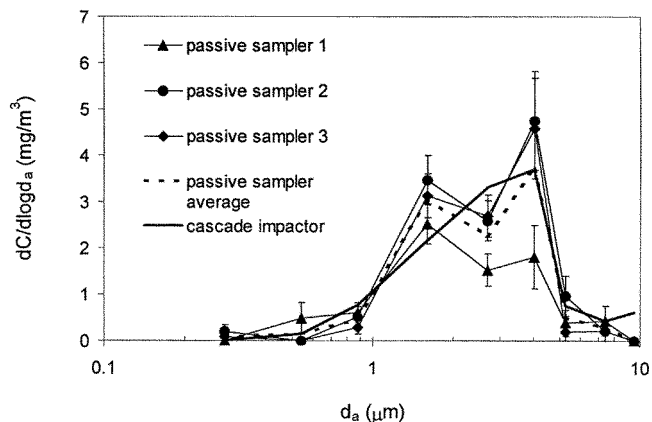


Figure 5. Typical results for one experiment: normalized concentration, $dC/d \log d_a$, vs. aerodynamic diameter, d_a , for three passive samplers and an impactor. The average of the three passive samplers’ results is also shown.

erally yielded OP values that were only minor improvements given their added complexity. In addition, these improvements would likely be offset in practice by the uncertainty in estimating u_* . For these reasons, Equation (6) was judged to be the best expression for γ_m .

Size distributions were then calculated for all experiments using Equations (1) and (6). The results for one experiment are shown in Figure 5. The error bars represent counting error only and were calculated with Poisson statistics.

Figure 6 shows the average passive sampler result for each experiment plotted against the corresponding impactor result. Results are plotted for PM2.5, PM10, mass median aerodynamic diameter (MMAD), and geometric standard deviation (GSD).

To determine sampler precision, a PROC NESTED analysis (SAS, Cary, NC) was performed on the natural logarithms of the passive sampler measurements. This analysis yielded the “within-experiment” variation due to differences among the

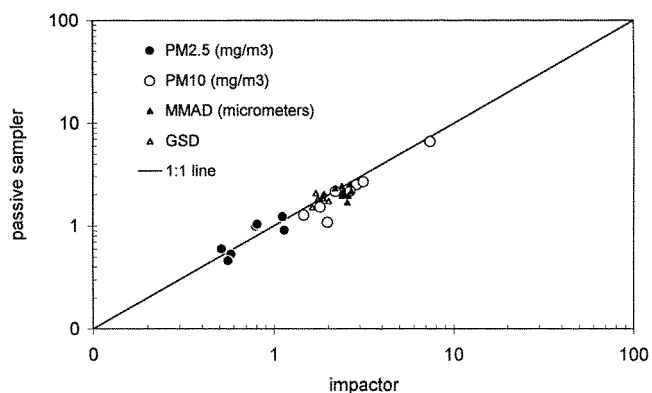


Figure 6. PM2.5, PM10, mass median aerodynamic diameter, MMAD, and geometric standard deviation, GSD, as measured by the passive samplers and impactor in the eight wind tunnel experiments.

three samplers in each experiment. The resulting CVs for PM_{2.5} and PM₁₀ were 18.1% and 32.2%, respectively. No consistent patterns were found in the variation between the left, center, and right passive sampler locations. Blank samplers exhibited negligible amounts of SiO₂ for all experiments.

Passive sampler size distributions were found to be approximately lognormal. Regressions for cumulative log-probability plots of the passive results yielded $R^2 = 0.93\text{--}0.98$, slightly lower than those determined for the impactor. Because of their lognormality, these size distributions can be adequately summarized in terms of their MMADs and GSDs.

DISCUSSION

Accuracy

To evaluate whether accuracy depended on particle size, mass concentration, wind speed, or RH, the results of the three passive samplers in each experiment were averaged. Analysis of variance (ANOVA) was performed on $\% \text{ error}_{(dC/d \log d_a)}$ to see if particle size was a significant effect. Again, data points that represented an average of < 1 count per sampler were discarded, as were comparisons where zero mass was recorded by the impactor. The dependence of $\% \text{ error}$ on particle size was found to be insignificant at the 0.05 level ($p = 0.07$).

Wind speed, RH, and concentration were found to be confounders with respect to one other. Thus ANOVA tests performed on each of these quantities were controlled for the other two. ANOVA revealed no significant dependence of $\% \text{ error}_{\text{PM}_{2.5}}$ and $\% \text{ error}_{\text{PM}_{10}}$ on wind speed (all p values > 0.5). No dependence of $\% \text{ error}_{\text{PM}_{2.5}}$ or $\% \text{ error}_{\text{PM}_{10}}$ was found on impactor PM₁₀, the index used for aerosol concentration level (all p values > 0.9). As to be expected with a nonvolatile aerosol, ANOVA showed no significant dependence of these quantities on RH (all p values > 0.6).

No significant variation of $\% \text{ error}_{\text{MMAD}}$ or $\% \text{ error}_{\text{GSD}}$ was found with wind speed, concentration level, or RH (all p values > 0.3).

Precision

As in the previous section, ANOVA tests of wind speed, RH, and concentration were each controlled for the other two. Figure 7 shows CVs for the three passive samplers in each wind tunnel experiment, calculated for PM_{2.5} and PM₁₀ and plotted against wind speed. Although this plot suggests decreasing trends in $\text{CV}_{\text{PM}_{2.5}}$ and $\text{CV}_{\text{PM}_{10}}$ with increasing wind speed, these trends are not statistically significant when one controls for concentration and RH (all p values > 0.3). Similarly, the ANOVA tests revealed no significant variation of $\text{CV}_{\text{PM}_{2.5}}$ or $\text{CV}_{\text{PM}_{10}}$ on concentration level (all p values > 0.07) or RH (all p values > 0.7).

Some of the between-sampler variation may have been due to small physical differences between each mesh cap. The precision is also dependent on the strength of the analysis technique, which is in turn heavily dependent on counting statistics. Be-

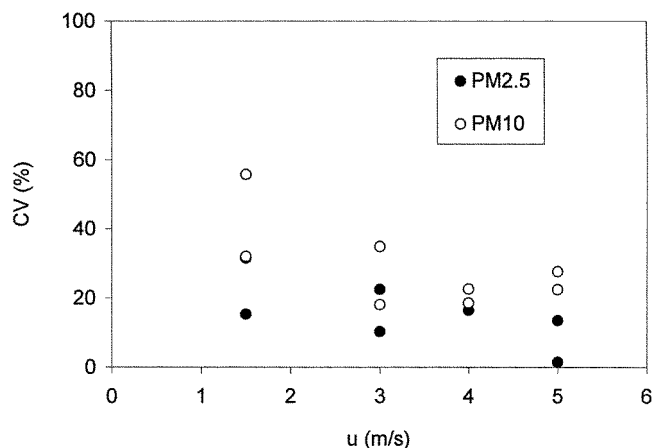


Figure 7. Coefficient of variation (CV) of collocated passive samplers for PM_{2.5} and PM₁₀ as a function of wind speed, u .

cause passive sampler counts were much lower than ideal, the sampler's precision is expected to improve under normal sampling conditions. Even so, the $\text{CV}_{\text{PM}_{2.5}}$ found here, 18.1%, is comparable to the EPA's stated objective of 15% precision for PM_{2.5} samplers (U.S. EPA 1996).

SENSITIVITY AND UNCERTAINTIES

The sensitivity of passive sampler results to particle density and shape factors was assessed with a representative wind tunnel data set. Table 3 shows the effect of $\pm 10\%$ changes in ρ_p , S_d , and S_v , on the average PM_{2.5}, PM₁₀, MMAD, and GSD. The tabulated numbers represent the average of the changes in the plus and minus directions. The effect of all factors on the GSD was negligible, while the effect of ρ_p and S_d on PM_{2.5}, PM₁₀, and MMAD was $< 10\%$. The results were quite sensitive to S_v , however, as $\pm 10\%$ changes produced a linear response in MMAD and changes in PM_{2.5} and PM₁₀ of 18 and 21%, respectively. Clearly, one must estimate S_v accurately. Using the techniques described by Wagner and Leith (2001), one should be able to estimate S_v to within about 10%.

Semivolatile particles are a potential source of error for the passive sampler. If SEM is used for analysis and the sample is placed under vacuum, the aerosol's volatile components will evaporate. By analyzing only the "dry" component of the aerosol, particle shape factors and densities will be incorrectly assessed and particle size will be underestimated. These errors cause

Table 3
Results of sensitivity analysis

Parameter	Percent change due to $\pm 10\%$ change in parameter:			
	PM _{2.5}	PM ₁₀	MMAD	GSD
ρ_p	± 3.6	± 5.2	± 6.5	∓ 0.5
S_d	± 6.5	± 4.9	∓ 6.5	± 0.6
S_v	± 18	± 21	± 11	∓ 0.4

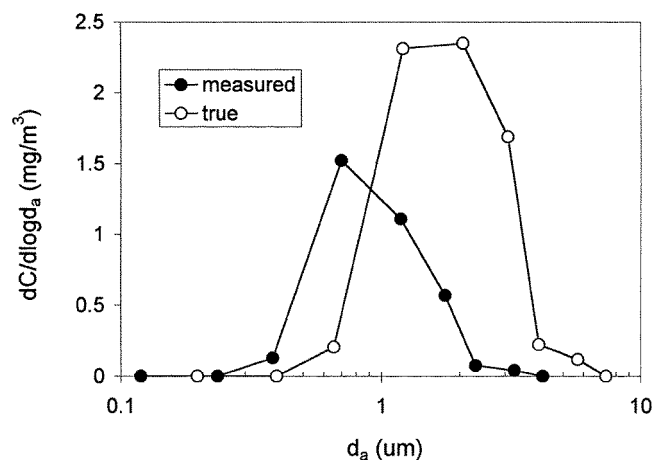


Figure 8. Simulated error when sampling an ammonium sulfate aerosol at 90% RH. Normalized concentration, $dC/d \log d_a$, vs. aerodynamic diameter, d_a .

underestimation of both the mass flux and deposition velocity, two deviations which counterbalance each other somewhat.

To assess the consequence of this situation, a sampling simulation was performed in which the particles were assumed to be ammonium sulfate collected at an average RH of 90%. This extreme scenario results in particles that are 75% water by mass. The simulated flux data were then analyzed in two ways. First, an ambient size distribution was calculated using only the dry-component flux, density, and shape factors. Second, a condensation equation accounting for curvature and solute effects (Seinfeld 1986) was used to calculate the "wet" flux at RH = 90%. The wet deposition velocity, density, and shape factors were then used to recalculate the ambient size distribution. The second result represents the "true" distribution, whereas the first represents the inaccurate, "measured" distribution derived from the dry component only (Figure 8). For this simulation, the errors for PM_{2.5} and PM₁₀ are 35 and 47%, respectively. The errors for MMAD and GSD are 46 and 1.5%, respectively. Because this is an extreme scenario, one would obtain much less error under more typical sampling conditions (i.e., lower mean RH or lower volatile aerosol fraction). If ambient-pressure analysis techniques such as atomic force microscopy are used instead of SEM, error would be reduced substantially. Nevertheless, one should be aware of this issue when passively sampling nitrates, organics, or hygroscopic particles. When using SEM, the passive sampler is best suited to applications that do not feature consistently high humidities or aerosols whose mass is dominated by volatile constituents.

These calculations suggest that a nonnegligible degree of measurement error is possible in some cases. However, temporal variability of concentrations is often much larger than these measurement errors (Rappaport 1994). This variability can result in significant errors in conventional long-term averages based on only a few short-term samples. Because the passive sampler effectively integrates over time, it eliminates this source of error and thus long-term averages measured by the passive sampler should generally exhibit better accuracy.

CONCLUSION

A wind tunnel has been developed to determine the empirical portion of the deposition velocity model and to test the precision of a passive aerosol sampler. The wind tunnel features an aerosol generator that can deliver polydisperse, nonvolatile dusts at high concentrations. The tunnel is relatively small, possessing a straight section 2.4 m long and inner dimensions of (50 × 100) mm. The reference sampler connected to the tunnel, an eight-stage impactor, is equipped with oleic acid-coated filter substrates to minimize particle bounce and an isoaxial, isokinetic probe. Aerosol concentrations were found to have a CV of <6% in the test section, while the diameter of average mass had a CV <1%. Friction velocities were found to range from 0.09 to 0.25 m/s for wind speeds of 1.5 to 5 m/s.

Wind tunnel tests of the passive sampler have determined a sampler precision of $CV_{PM_{2.5}} = 18.1\%$ and $CV_{PM_{10}} = 32.2\%$. The mesh correction factor, γ_m , was empirically determined by minimizing the sum of squares difference between impactor and passive sampler across all size bins and all experiments. The relatively simple correlation is a function of the particle Reynolds number only. ANOVA tests were conducted on accuracy and precision to see whether they depended on wind speed, RH, or aerosol concentration, and accuracy was tested with respect to particle size. No significant trends were observed. The volume shape factor was the most sensitive of the mass and shape conversion variables.

If SEM is used for analysis, the passive sampler will exhibit some error when sampling semivolatile aerosols. For this reason, the passive sampler is probably best suited to applications that do not feature consistently high humidities or aerosols whose mass is dominated by volatile constituents. If ambient-pressure analysis techniques such as atomic force microscopy are used instead of SEM, however, this source of error should be much less. Because the passive sampler integrates over hourly and daily fluctuations in concentration, it should be more accurate than conventional short-term samples when monitoring long-term exposures.

Work is currently underway to test the passive sampler in an occupational setting. These tests will provide a measure of the passive sampler's accuracy under actual, variable conditions.

ACKNOWLEDGMENTS

The authors wish to thank the National Institute for Occupational Safety and Health (1 R03 OHO3774-01), the U.S. Environmental Protection Agency (U-915321-01-0), the National Institute of Environmental Health Sciences (5 T32 ES07018-21), the U.S. Department of Education (P200A40274-96), and the UNC Board of Governors for supporting this work, Randall Goodman for his assistance with the wind tunnel design, and Dr. Robert Bagnell for his assistance with the SEM analysis.

REFERENCES

- Davies, C. N. (1979). Particle-Fluid Interaction, *J. Aerosol Sci.* 10:477-513.
- Ramachandran, G., Sreenath, A., and Vincent, J. H. (1998). Towards a New Method for Experimental Determination of Aerosol Sampler Aspiration Efficiency using Scaling Relationships, *J. Aerosol Sci.* 29:875-891.

- Rappaport, S. M. (1994). Interpreting Levels of Exposures to Chemical Agents. In *Patty's Industrial Hygiene and Toxicology, Third Edition, Volume 3, Part A*, edited by R. L. Harris, L. J. Cralley, and L. V. Cralley. John Wiley and Sons, New York, pp. 349-403.
- Schlichting, H. (1979). *Boundary-Layer Theory*, 7th ed., McGraw-Hill, New York, p. 603.
- Seinfeld, J. H. (1986). *Atmospheric Chemistry and Physics of Air Pollution*, John Wiley and Sons, New York, p. 349.
- Turner, J., and Hering, S. (1987). Greased and Oiled Substrates as Bounce Free Impaction Surfaces, *J. Aerosol Sci.* 18:215-224.
- U.S. Environmental Protection Agency (1996). Proposed Requirements for Designation of Reference and Equivalent Methods for PM_{2.5} and Ambient Air Quality Surveillance for Particulate Matter, *Fed. Reg.* 61:241, 65785.
- Wagner, J., and Leith, D. (2001). Passive Aerosol Sampler. Part I: Principle of Operation, *Aerosol Sci. Technol.*, (see preceding article in this issue).
- White, F. M. (1994). *Fluid Mechanics*, 3rd ed., McGraw-Hill, New York, p. 314.